remote sensing

MDPI

Article

How Phenology Shapes Crop-Specific Sentinel-1 PolSAR Features and InSAR Coherence across Multiple Years and Orbits

Johannes Löw [1,*], Steven Hill [2], Insa Otte [2], Michael Thiel [2], Tobias Ullmann [2] and Christopher Conrad [1]

[1] Department of Geoecology, Institute of Geosciences and Geography, Martin-Luther University Halle-Wittenberg, 06120 Halle (Saale), Germany
[2] Department of Remote Sensing, Institute of Geography and Geology, University of Würzburg, 97074 Würzburg, Germany
* Correspondence: johannes.loew@geo.uni-halle.de

Abstract: Spatial information about plant health and productivity are essential when assessing the progress towards Sustainable Development Goals such as life on land and zero hunger. Plant health and productivity are strongly linked to a plant's phenological progress. Remote sensing, and since the launch of Sentinel-1 (S1), specifically, radar-based frameworks have been studied for the purpose of monitoring phenological development. This study produces insights into how crop phenology shapes S1 signatures of PolSAR features and InSAR coherence of wheat, canola, sugar beet. and potato across multiple years and orbits. Hereby, differently smoothed time series and a base line of growing degree days are stacked to estimate the patterns of occurrence of extreme values and break points. These patterns are then linked to in situ observations of phenological developments. The comparison of patterns across multiple orbits and years reveals that a single optimized fit hampers the tracking capacities of an entire season monitoring framework, as does the sole reliance on extreme values. VV and VH backscatter intensities outperform all other features, but certain combinations of phenological stage and crop type are better covered by a complementary set of PolSAR features and coherence. With regard to PolSAR features, alpha and entropy can be replaced by the cross-polarization ratio for tracking certain stages. Moreover, a range of moderate incidence angles is better suited for monitoring crop phenology. Also, wheat and canola are favored by a late afternoon overpass. In sum, this study provides insights into phenological developments at the landscape level that can be of further use when investigating spatial and temporal variations within the landscape.

Keywords: crop monitoring; agriculture; C-band; open data cube; growing degree days

Citation: Löw, J.; Hill, S.; Otte, I.; Thiel, M.; Ullmann, T.; Conrad, C. How Phenology Shapes Crop-Specific Sentinel-1 PolSAR Features and InSAR Coherence across Multiple Years and Orbits. *Remote Sens.* **2024**, *16*, 2791. https://doi.org/10.3390/rs16152791

Academic Editor: Liang Sun

Received: 21 May 2024
Revised: 12 July 2024
Accepted: 27 July 2024
Published: 30 July 2024

1. Introduction

In recent years, the concept of essential variables (EVs) has been introduced to assess progress towards Sustainable Development Goals across policy domains [1]. EVs that capture the progress of the agricultural domain are currently defined by the Group on Earth Observations Global Agricultural Monitoring (GEOGLAM) [2]. In this catalogue, phenology—more specifically, the current crop stage—is listed as an EV. It has been established that phenology provides crucial information for crop management because it strongly relates to plant productivity and growth. Furthermore, certain stages of the crop lifecycle are highly sensitive to meteorological conditions [3–6]. In the context of an increasing frequency of and more extreme weather events, as well as complex topics such as climate adaption and resilience, this kind of information is in high demand [7–9]. Consequently, Earth observation data and products have been widely researched in the field of agriculture as a potential source of such information. This field has been dominated by multispectral optical sensors such as Landsat or the Moderate Resolution Imaging Spectroradiometer (MODIS) for a long time. However, spaceborne synthetic aperture radar (SAR) data have been researched increasingly during the last decade, either as an additional or an alternative

data source, as SAR provides textural or structural instead of spectral information and it is independent of weather and illumination conditions [8,10]. More specifically, the start of the European Sentinel-1 mission in 2015 caused an increase in research activities using SAR data for various applications [9,11,12]. In the context of tracking crop phenology, three major forms of analysis have been established: machine learning classifiers, such as random forest or deep learning [13,14], stochastic or statistical modeling [15,16] and time series metrics (TSMs) [17–19].

The study at hand focuses on TSMs, more specifically extreme value and break point analysis. For description, a crop phenology classification scheme has been established by Biologische Bundesanstalt für Land und Forstwirtschaft, Bundessortenamt und CHemische Industrie (BBCH) The BBCH scale categorizes plant growth according to micro and macro stadia [20]. In this case the phenological development of the following crops is tracked: wheat, sugar beet, canola, and potatoes. These crops cover a wide range of physiognomic properties and management requirements (e.g., irrigation of potatoes); thus, a more general assertion can be framed. Hence, this study offers a wider perspective of the signal–target interaction during the crop lifecycle than studies that focused only a specific crop type or crop family [15,17,21]. Moreover, the addition of InSAR coherence (hereafter referred as "coherence") to polarimetric features, as suggested by Lobert et al. [14], might lead to improvements in monitoring crop phenology, since coherence might be more sensitive to early stages of the plant lifecycle due to the temporal decorrelation of the signal caused by the emergence of crops. In the context of a multiannual approach, we also address the dilemma outlined by Harfenmeister et al. [22] that the chronological occurrence of TSMs, especially break points, cannot be reliably used to allocate phenological development by SAR time series. Hence, we introduce agrometeorological data, namely, growing degree days (GDDs) [23], as an artificial baseline for calibrating and validating the occurrence of TSMs and their associated progress of plant growth. GDDs contribute to the assessment of reliability by adding information on thermal growth potential to the occurrence of TSMs. Apart from these gaps, the mission ending malfunction of Sentinel-1B produced a new aspect: integrating multiple orbits to conserve a comparatively dense time series. As of January 2022, it is no longer possible to rely on the six-day repetition rate, provided by the twin constellation [24] over our study area. Hence, we used data from the existing archive to track phenological development simultaneously across different orbits. Recently, such an idea was addressed over wheat fields and sunflower plantations [25–27], but the focus was either on deriving biophysical parameters or investigating the intensity of the backscatter only. Hence, this study aims at generating information regarding if and how these orbits differ in their response towards phenological development of multiple crops and S1 InSAR and PolSAR features. The current assumption is a negligible difference as soon as there is a certain volume of biomass on the fields [13,25–27].

Since all of the abovementioned issues are highly dependent on how the respective time series are generated, and especially on the usage of smoothing algorithms and their parametrization, a density-based framework across multiple parametrizations of a single smoothing algorithm is used in this study. Such stacking of different degrees of smoothing helps to mitigate the inevitable loss of information of highly smoothed time series. Thus, entire periods, instead of points, which cause a phenologically induced signal change, are revealed. The fundamental hypothesis of such an approach is as follows: extrema and break points, which originate from events that drastically shape a crop-specific time series, remain visible throughout various intensities of smoothing.

Here, we employed the frequently used "locally estimated scatterplot smoothing" (LOESS). This decision was based on two factors. Firstly, Cai et al. (2017) [28] stated that there is no mayor difference between locally weighted smoothing techniques. Secondly, commonly applied smoothing techniques in studies related to phenology are locally weighted (e.g., Whittaker [29], Savitzky-Golay [30], LOESS [17,18]). Considering the stacking of different smoothing degrees and the small differences between the individual algo-

rithms, it is assumed that our approach produces representative crop signatures, despite employing only LOESS.

In sum, this study addresses the following issues centered around crop monitoring via SAR time series: (i) combining information obtained from time series of different smoothing intensities [28] (ii) as well as different S1 viewing geometries, ergo, relative orbits in a singular conceptual framework without angle normalization. Furthermore, (iii) the variance in chronological occurrences of break points and extreme values [21] is investigated. This study addresses these issues by (i) estimating the density of TSM occurrences by stacking time series of different smoothing intensities at the field level and aggregating the findings to derive landscape-wide (the extended DEMMIN site covering an area of 25 km by 25 km) patterns. Here, the time series analyses are conducted separately for each orbit generating insights into (ii) orbit-related discrepancies within the patterns at landscape level. In regard to the issue of chronological occurrence, a GDD baseline is introduced for calibration and validation. This provides a temporal coordinate system consisting of day of year and thermal growth potential. Because this approach aims at generating systematic insights into the relationship of crop phenology and the inherent randomness of SAR signals [31], the study encompasses seven S1 features, three relative orbits, and an observation period of five years [31].

2. Materials and Methods

2.1. Study Area, and In Situ Data

The area of interest is located in northeastern Germany in the federal state of Mecklenburg West Pomerania (Figure 1, MV). An average annual precipitation of 550 mm and perennial humidity in combination with a mean air temperature of 8.3 °C designate its climate as temperate Middle-European [32]. The study area surrounding the Durable Environmental Multidisciplinary Monitoring Information Network (DEMMIN) is characterized by a low elevation gradient of ca. 120 m, because its landscape is dominated by ground moraines. Such terrain of low complexity is ideal for SAR-based analysis, because the terrain is less likely to cause signal interferences [33]. Information on parcel delineation and crop type in the DEMMIN area were extracted from a dataset of the German integrated administration and control system (InVeKoS) of Mecklenburg West Pomerania for the civil years of 2017 to 2021. In regard to crop type, the data were assembled for wheat, sugar beet, canola, and potatoes. The InVeKoS-framework separates starchy potatoes from other potatoes [34], but for the purpose of this study, this distinction was deemed noncritical in relation to the phenological development. Additionally, only parcels of a relevant size were selected to minimize the influence of pixel contamination by neighboring land use or cover [14]. The thresholds for relevant sizes were set to 3 ha for wheat, canola, and sugar beet and 2 ha for potatoes because there are significantly less fields above 3 ha where potatoes were cultivated. For each year, around 550 fields of wheat, 350 fields of canola, 150 fields of sugar beet, and 10 fields of potato were observed.

Phenological in situ observations were available from the voluntary-based observer framework of the German weather service (DWD) [35]. As the area of interest is poorly covered by this monitoring setup, the average occurrence date by federal state was used as a source for validation data in combination with the corresponding GDD summation. Any phenological developments that were recorded by DWD were translated to the BBCH [20] scale to enable a comparison with other studies that also use this classification scheme for measuring the progress of crop lifecycles. The translation and assignment of DWD observations to crop types and BBCH codes resulted in a list of phenological stages, shown in Table 1.

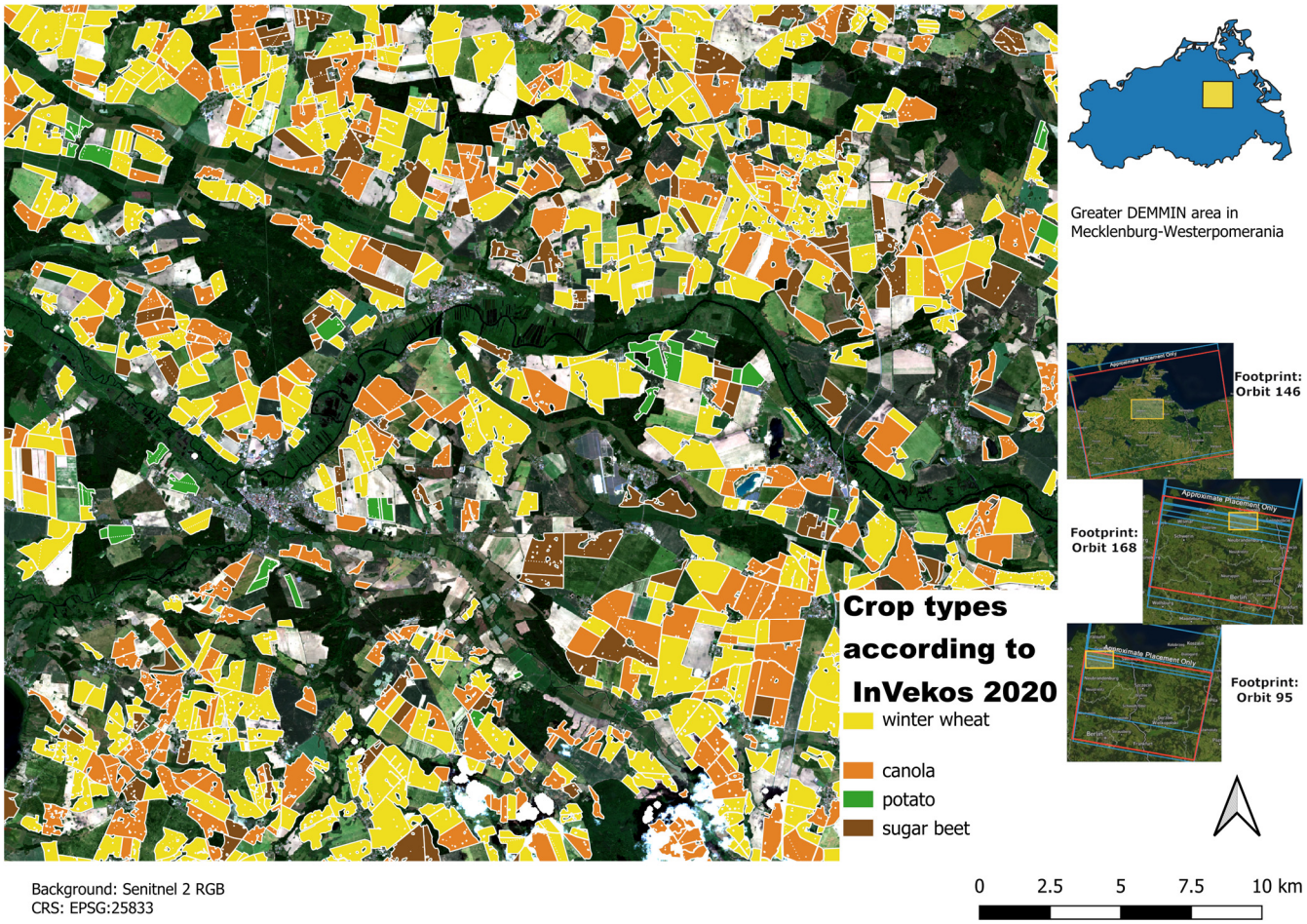

Figure 1. Map of InVeKoS data 2020 for DEMMIN and the selected crops: winter wheat, sugar beet, canola, and potato. Top right corner: extent of the AOI in Mecklenburg Western Pomerania. Center right: extent in relation to footprint of relative orbits.

Table 1. Translation of phenological stages into BBCH codes by crop type.

Phenological Development	BBCH Code	Crop Types
Germination	0	Sugar beet, potato
Leaf development	10	Sugar beet, potato
Stem elongation	30	Winter wheat
Canopy closure (90%)	39	Sugar beet, potato
Heading or inflorescence	50	Winter wheat, winter canola
Flowering	60	Winter canola
End of flowering	69	Winter canola
Yellow ripening	87	Winter wheat
Harvest	99	Winter wheat, canola

The authors are aware of potential limitations with regard to observation periods corresponding to civil years and availability of in situ data. Therefore, references to BBCH 0 and BBCH 10 for winter crops serve as general points of orientation within phenological progress of the civil year and not as actual validations to the onset of the actual stage of winter crops. It marks the likely start of the next growing season and, thus, a likely end of cultivation of catch crops. This is necessary to identify phases that are more vulnerable to noise or strong variations such the growing period of catch crops, varying soil management practices regarding, for example, stubble fields and straw covers.

2.2. Growing Degree Data

Growing degree is defined as the number of temperature degrees above a certain threshold base temperature and is a commonly used tool to describe the development of biological processes, including crop phenology [23]. The integral (summation) of these numbers over a day is used to describe crop growth for that specific day, generating a growing degree day, or GDD. By assigning a GDD value to each TSM occurrence and in situ observation, the idea behind crop maturity can then be used to describe progress in subsequent analysis of the results of this study.

Nevertheless, there has always been some criticism that this linear relationship does not consider an upper temperature limit of plant growth, consequently leading to artefacts, especially when extreme temperatures and variable conditions are observed [36–38]. Hence, a more complex method is chosen in this study, which was proposed by Zhou and Wang (2018) [38] to account for these shortcomings. Our observation period contains years of extreme drought in Germany [17,21]; thus, selecting a more sophisticated method was deemed necessary. In this case, an hourly temperature time (*HTT*) is calculated and it encompasses four parameters: T_u is the upper limit of temperature above which no plant growth is assumed due to intense heat stress. T_{opt} is the optimal temperature, where maximum growth occurs, and T_{base} is the base temperature that is needed to induce growth. Finally, T_h represents the hourly measurement of air temperature [38].

$$HTT = \begin{cases} 0, & T_h < T_{base} \\ \left[\frac{T_h - T_{base}}{T_{opt} - T_{base}}\right]\left[\frac{T_u - T_h}{T_u - T_{opt}}\right]^{\frac{T_u - T_{opt}}{T_{opt} - T_{base}}} & T_{base} \leq T_h \leq T_u \\ 0, & T_u < T_h \end{cases} \quad (1)$$

The actual data on air temperature, which is measured two meters above ground and provided by DWD for 2017–2021, were acquired as an interpolated raster derived from the agrometeorological network of DEMMIN. The native spatial resolution of the dataset is 250 m × 250 m per pixel, its temporal resolution is one hour, and it was interpolated by employing ordinary kriging. Further details are provided by the DWD [39].

The GDD time series is the sum of daily mean of HTT (see Equation 2) over a specific timeframe (e.g., growing season or civil year). Furthermore, the GDDs constitute the second layer of validation data, because each occurrence of a TSM and each in situ observation are linked to their corresponding GDD values. Hereby, the distance between in situ observations and TSM occurrence is also described by the difference in thermal potential of plant growth. The calculations of corresponding GDD values are conducted on an open data cube platform (ODC) [40,41] using Python. Table 2 lists the specification of all the thresholds of temperature by crop type. These specifications were derived from the literature, which is also included in the table.

Table 2. Specifications of lower (T_{base}), optimal (T_{opt}), and upper (T_U) thresholds of air temperature with regard to plant growth and calculating HTT.

Crop Type	T_{base}	T_{opt}	T_U	References
Winter wheat	0	21	31	[42,43]
Winter canola	4	25	34	[44]
Sugar beet	7	24	32	[45,46]
Potato	5	22	30	[47,48]

The artificial baseline and the civil year were, as mentioned in the introduction, a deliberate choice. Not only does this enable the discovery of trackable pre-/post-season events, but also it corresponds to statistical records at the federal or national level as well as with the budgeting of state-run institutions in addition to the fiscal year.

Because the yearly observation periods of this study are civil years, the start of the GDD summation was set to 1 January in each year. Hence, GDDs are used as an artificial baseline that offers information on phenological developments based on their thermal growth potential. Therefore, GDD values are not used in a classical, absolute way to model plant growth [49]. Instead, they are used as an artificial progress bar (GDDsim) of a year to calibrate and validate the occurrences of TSMs. This is based on the principle of crop maturity [15] and the idea that relative progress towards BBCH stages can be described by their respective GDDsim values. Moreover, by using DOY and GDDsim, a temporal coordinate system was established to allocate and evaluate timeframes of phenologically induced signal change.

2.3. Sentinel-1 Time Series

The time series of S1 data, which includes relative orbits 146 (ascending) and 95 and 168 (descending), encompasses the years of 2017 to 2021 and amounts to around 1050 images in total. Because break point analysis and the search for phenologically relevant extrema require calibration periods before and after an event of interest [22], it was decided to extend yearly observations to the civil year. Thus, it was ensured that no phenological development was lost during the calibration phase of the analysis. Additionally, first indications of the trackability of pre- and post-growing season events could be derived. An overview of orbit IDs, their viewing geometry, and the respective range of incidence angles are listed in Table 3.

Table 3. Summary containing range of incidence angles covering the study area, times of overpass, and flight directions of each relative orbit.

Relative Orbit ID	Flight Direction	Min. Incidence Angle (°)	Max. Incidence Angle (°)	Local Time of Overpass
146	ascending	30	41	16:52
168	descending	30	41	05:24
95	descending	41	45	05:16

All datasets were acquired in interferometric wide swath mode (IW) and VV/VH polarization. Because interferometric and polarimetric features were calculated, single look complex (SLC) [50] was chosen. A combination of the Python library pyroSAR [51], which provides a parser for the XML-based graph builder, and SNAP (Version 9) was used to preprocess the data. This was also integrated in an ODC environment [41], which served as a cloud-based data management and computation platform. The processing chain for polarimetric features contains terrain flattening [33], multilooking with one look in azimuth and four looks in range, speckle filtering by a 5 pixel $\times$ 5 pixel boxcar filter, and a range-Doppler terrain correction [52], resulting in a 20 m $\times$ 20 m spatial resolution and gamma nought (GN) backscatter. Since backscatter was scaled to dB, the cross-polarization (CR) ratio was calculated by VV-VH. Alpha (h2a_alpha) and entropy (h2a_entropy) were derived from a C-2 Matrix [53]. As for the interferometric (InSAR) coherence, parameters for multilooking and terrain correction remained the same. The calculation of the coherence included the removal of the flat Earth and topographical phase by a moving window of three pixels in azimuth and eleven pixels in range as well as a six-day temporal baseline and consecutive master images [54]. Shuttle Radar Topography Mission (SRTM) data (1 arc-second) were used in all steps requiring a digital elevation model. This set of S1 features, consisting of VV/VH backscatter intensity, CR, h2a_alpha, and h2a_entropy, as well as VV/VH coherence, has been proven to reflect the changes in plant physiognomy along the crop lifecycle by various studies [17–19,22,30].

2.4. Multiorbit Time Series Analyses

The framework of this study combines two spatial scales: the field (i.e., micro) level and the landscape, i.e., a region or any other artificial or (natural) stratum. Here, the latter refers to the extent of the DEMMIN test site. An overview of the essential steps is provided in Figure 2. These steps were conducted separately for each year, SAR feature, and relative orbit of the S1 dataset to provide insights into the temporal patterns of a combined orbit approach. Details on these steps are presented in the subsequent chapters.

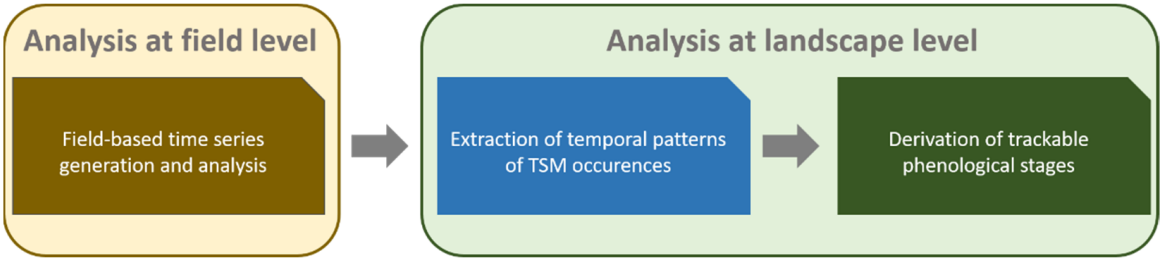

Figure 2. Essential steps of the analysis per orbit and year separated by field and landscape level.

2.4.1. Field-Based Time Series Generation and Analysis

As mentioned in the introduction, a core hypothesis of this study is that phenologically induced changes of the crop signature remain prevalent across multiple parametrizations of a smoothing algorithm [17,18]. In the case of this study, LOESS with tri-cubic weight and one-degree polynomial regression [17] was employed [55]. When applying LOESS, the span is the parameter, by which the magnitude of smoothing is substantially changed.

Field-based time series generation encompasses three steps: (i) Applying a sequence of spans ranging from 0.05 to 0.5 in steps of 0.05. This range covers the majority of smoothing scenarios from "close to raw data" (0.05) to "strongly oversmoothed" (0.5). (ii) Detection of TSMs, in this case., break points [56,57], as well as maxima and minima in smoothed time series. (iii) Generation of TSM occurrence plots with a common bin size of six days (akin to the revisiting rate of S1) were generated for the derivation of TSM occurrences at the respective field. Such an operation stacks and unifies the indicated break points as well as maxima and minima into single series for each TSM (see below). This particular part of the framework is shown in Figure 3. The figure depicts the generation of a TSM occurrence plot at the field level, the type of S1 features and crops, as well as the respective relative orbits and years covered by this study.

This intermediary result is a TSM occurrence plot, illustrating the major windows of phenologically induced signal change on field level. The TSM occurrence plots for the extrema were generated separately for minima and maxima. Exemplary, yearly signatures of each crop type, in this case VV intensity, and their respective extreme values are shown in Figure 4.

When working with SAR time series in the context of crop monitoring, a high number of noise-induced extrema can be introduced due to stochastic movement of plants or weather events such as rainfall or strong winds. Weakly smoothed time series are especially sensitive to such sources of noise. Therefore, a filter based on the standard deviation along the temporal dimension was introduced. This filter excludes sequences of extrema, where the difference between individual extreme values does not exceed the standard deviation. The filter was applied to reduce the count of non-phenologically relevant extrema (i.e., variations exceeding one standard deviation were removed). Similar measures are also found in other studies [18,30].

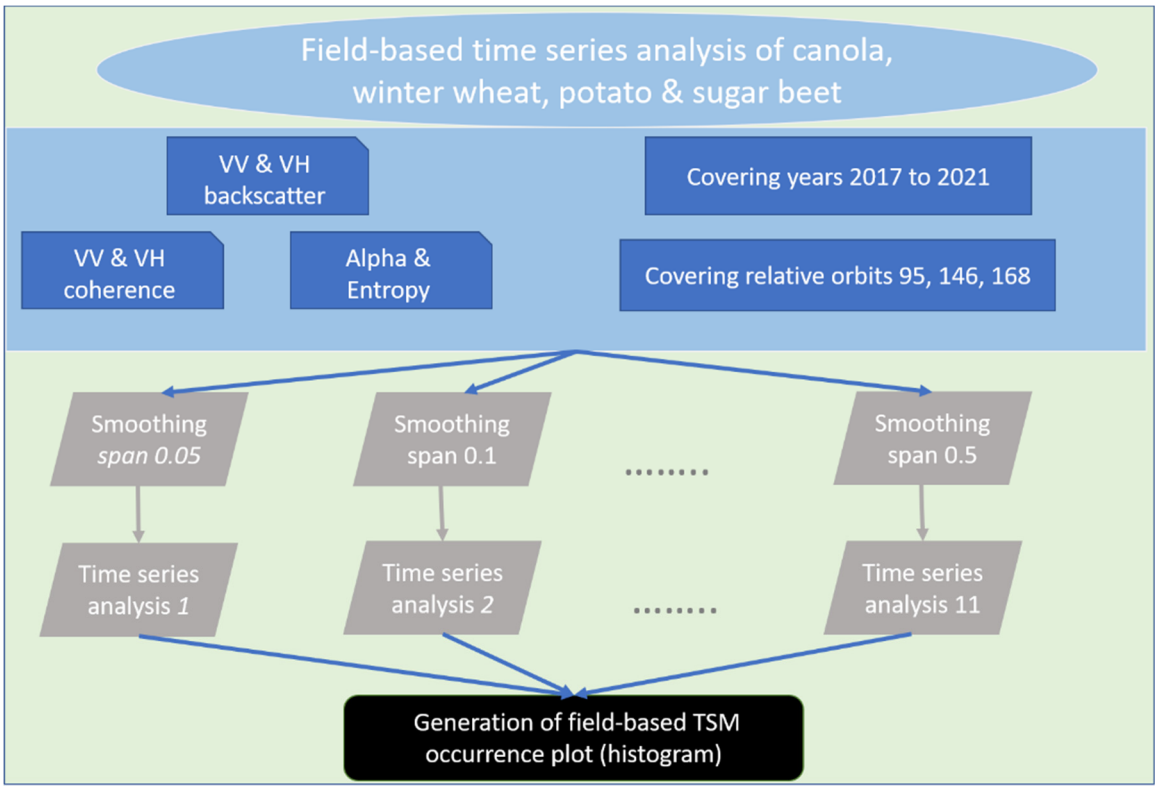

Figure 3. Schematic depiction of estimating temporal density (TSM occurrence plot) of TSM occurrence at the field scale. The dimensions of content of the analysis encompass five years (2017–2021), three relative orbits (146,168, 95), and seven S1 features. The smoothing span ranges from 0.05 to 0.5 in steps of 0.05, resulting in eleven (n = 11) time series per field.

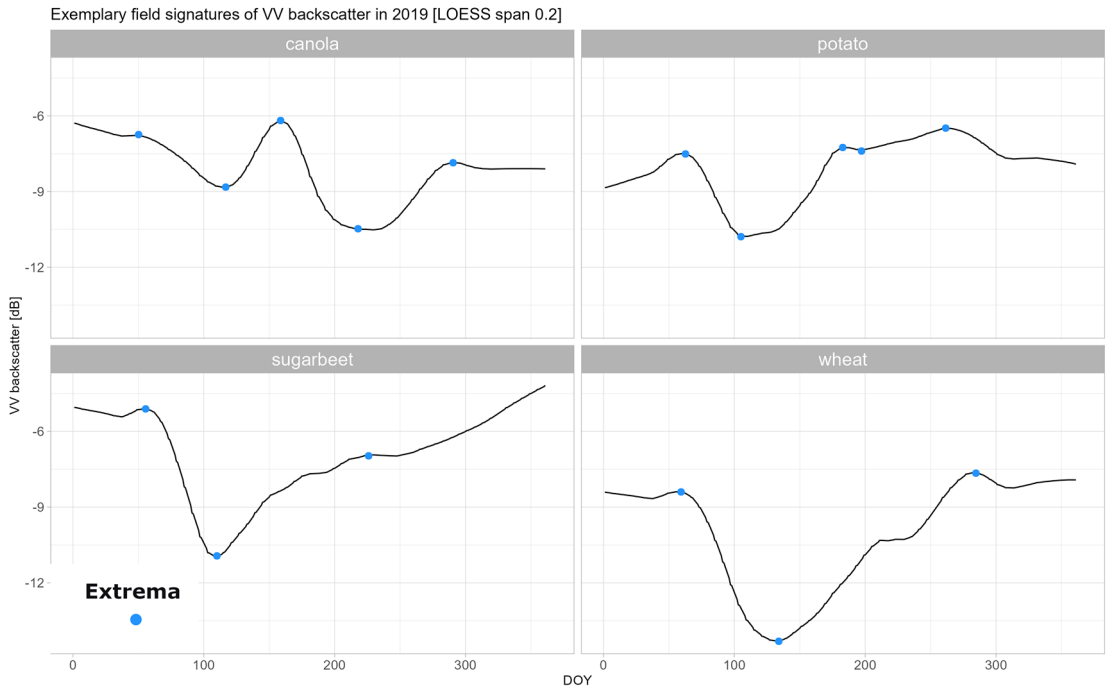

Figure 4. Exemplary yearly crop signatures for each crop type of VV backscatter with locations of their extrema. Signatures were smoothed by LOESS with span 0.2.

2.4.2. Extraction of Temporal Patterns in TSM Occurrences at the Landscape Level

In the second step (Figure 2), TSM occurrence plots were generated at the landscape level for each crop type. They display the overall distribution within the targeted area. Since only greater densities of occurrence are of interest, a threshold-based approach was used to decide which number of occurrences per field is considered a substantial amount. This threshold is calculated automatically for each crop type, orbit, year, S1 feature, and TSM by the sum of the mean and standard deviation of all counts of occurrences that are not zero. Furthermore, this is also conducted separately for each field in every year. Thereby, the relevance of TSM occurrences was assessed relative to the growing conditions of a year and the crop- and orbit-specific effects, and the sensitivity of the S1 features to changes during the crop lifecycle were considered. Figure 5 displays the general framework of the analysis at the landscape level.

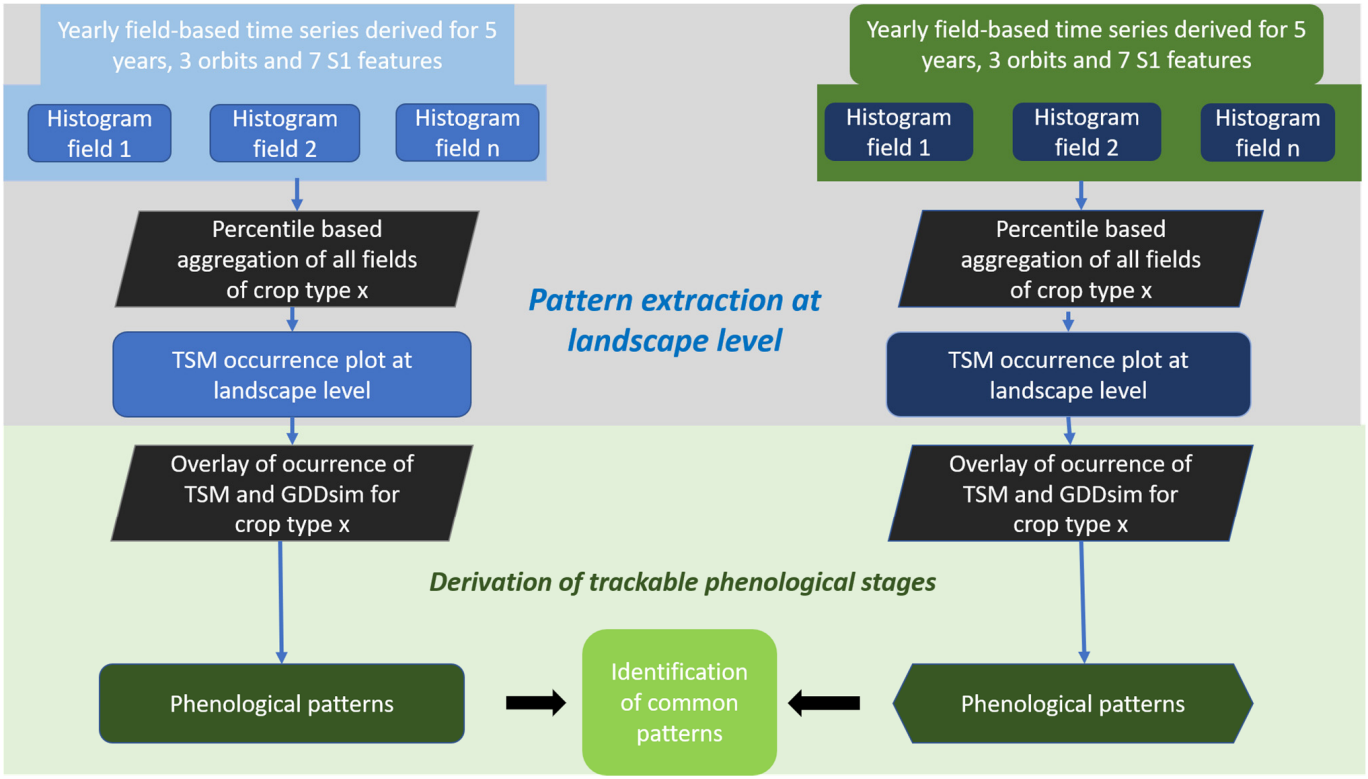

Figure 5. Schematic depiction of the analyses at the landscape level containing the pattern extraction and the derivation of trackable stages. This was applied for time series originating from different years and/or orbits of the same crop type and S1 feature to enable the comparison of their respective TSM distributions. These comparisons allow for the derivation of common phenological patterns across years and orbits for each crop type and S1 feature.

As illustrated by Figure 5, the last step of the pattern extraction at the landscape level encompasses an overlay of TSM occurrences with the crop-specific GDDsim baseline Thereby, any substantial occurrence of a TSM was assigned to its corresponding range of GDDsim values.

2.4.3. Derivation of Trackable Phenological Stages

The derivation of trackable phenological stages was accomplished by comparing the date of occurrence for TSM (tracked) with the dates recorded by DWD (observed). Such a comparison enables the allocation of phenological stadia by either matching tracked TSM with the closest DWD observation by difference in days and GDDsim, i.e., $DOY_{tracked}$–$DOY_{observed}$ or $GDDsim_{tracked}$–$GDDsim_{observed}$. In a subsequent step, these

differences were then used to evaluate the tracking crop-specific performance of S1 for each orbit, year, and S1 feature.

Therefore, differences between in situ observations and tracked events were aggregated by mean and standard deviation across all five years for each orbit, S1 feature, and phenological stage. The computation of mean values generated insights into the general tendencies of temporal offsets (earlier or later than in situ observation) and the standard deviation is calculated to measure the variance of these mean temporal offsets. By imposing a threshold of ten days, or 150 GDDsim on the standard deviation, the reliability of TSMs derived from an S1 feature was assessed according to its temporal variation across the five years. The threshold of ten days was defined to resemble the S1A and S1B repetition rates of a single platform and according to offsets commonly found in the literature [17,21,27]. With a temporal threshold of 10 days, the corresponding threshold of GDDsim was set to 150 assuming a daily accumulation of 15 GDDsim, which coincides with a value of solid growth potential fitting all investigated crops. This is based on the concept of crop maturity, which states that each BBCH stage has a corresponding average GDDsim value [15]. Hence, each TSM occurrence close to that corresponding GDDsim value is most likely caused by its associated BBCH value. Furthermore, the reliability for the stages represented within the DWD observations was determined by applying an additional threshold of twelve days (akin to the repetition rate of a single S1 platform) on the mean offset between TSM patterns and in situ observations. The aggregation by orbit serves as an indicator as to which viewing geometry more likely to produce TSMs close to the targeted stages. The aggregation by BBCH stage, on the other hand may reveal parts of the crop lifecycle, where the tracking capabilities of this framework are limited. Finally, the aggregation by S1 features highlights those S1 features whose TSMs patterns are most suited for tracking certain stages of crop development [58].

3. Results

3.1. Major, Phenologically Induced Changes in Crop-Specific Time Series

The first objective of this study focused on the major changes in crop- and orbit-specific signals. By aggregating the occurrence of TSMs via threshold to the landscape level, a general pattern was made visible. To check if these patterns represent season-specific dynamics, an exemplary subset of the pattern derived by break points is illustrated in Figure 6. Here, the patterns of relevant TSM occurrences for winter wheat in 2018 and 2020 are displayed by their corresponding GDDsim (y-axis) and DOY (x-axis) values. Furthermore, the vertical and horizontal lines of different style represent BBCH stages according to their mean GDDsim and DOY values over five years. At first glance, the combination of all S1 features covers the targeted BBCH stages as well as stages before BBCH 30 (stem elongation) and during the time between BBCH 99 (harvest) and BBCH 0 (germination). By comparing the two years, four major patterns emerge. (i) Firstly, the distribution of 2020 (blue dots) is more compact across all S1 features. (ii) Secondly the wider distributions in 2018 often show orbit-specific tendencies, whereas 2020 mostly exhibits windows of change originating from multiple orbits. (iii) Thirdly, 2018 and 2020 appear to be on different progressions of GDDsim summation. (iv) Fourth, depending on the year, certain unique patterns emerge or stages are only covered in one of the two years (e.g., intensity_cr and h2a_alpha: BBCH 87).

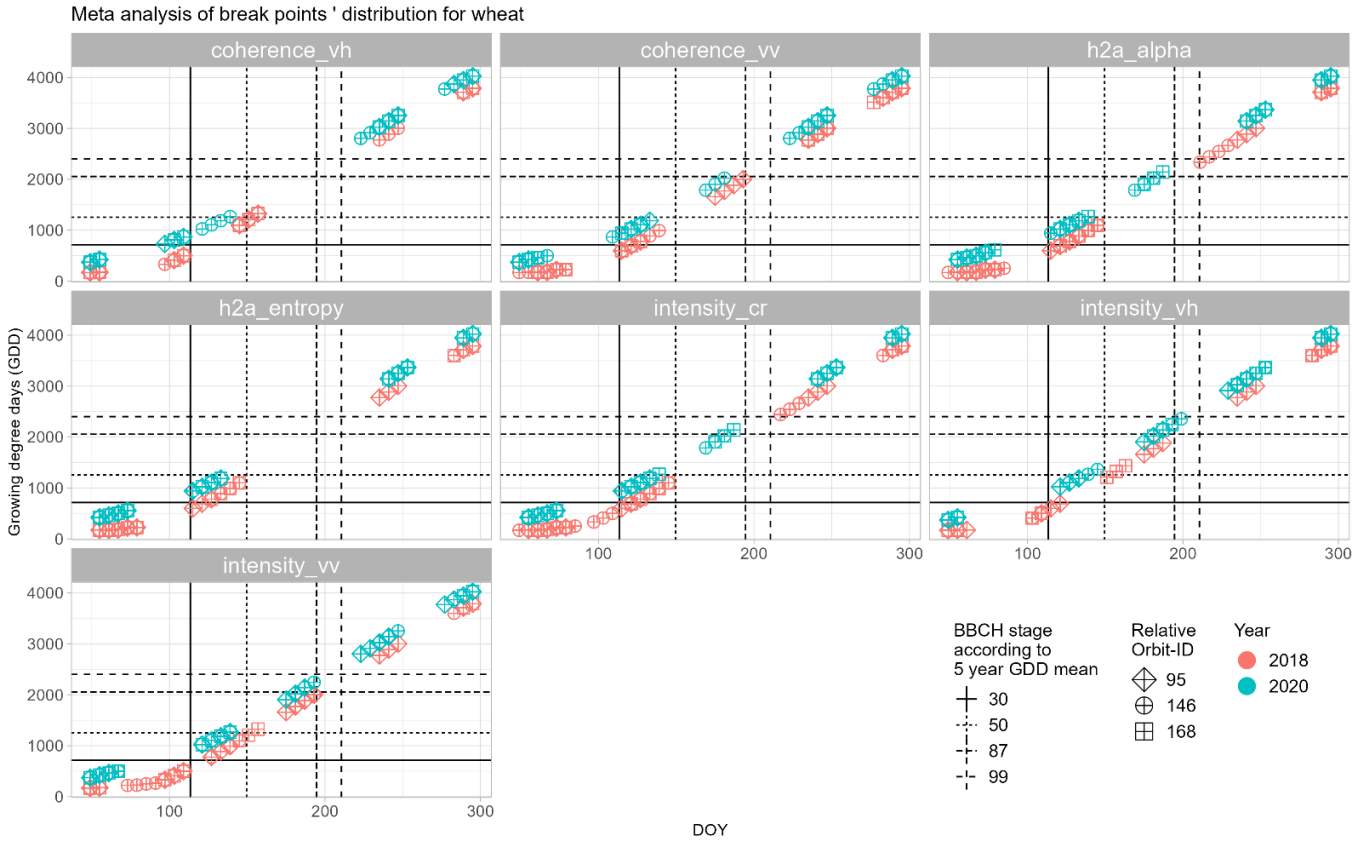

Figure 6. Orbit-specific patterns of major signal changes at landscape level tracked by break points according to day of year (DOY; *x*-axis) and artificial growing degree day (GDDsim) values (*y*-axis) in relation to the corresponding five-year mean GDDsim value of BBCH stadia observed by DWD at landscape level from 2018 and 2020. Exemplary illustration for fields of wheat. Temporal uncertainties around BBCH stadia are marked by grey areas. Exemplary illustration for fields of winter wheat.

These patterns remain visible to a large degree when observing the distributions of break point occurrences across the entire observation period, which are depicted in Figure A1. While the individual progression is harder to track by visual interpretation, the major time slots of phenologically induced signal change can be found for each S1 feature. The in situ observations are covered by a combination of all features, and additional windows of signal change for break points were discovered around 250 GDDsim (before stem elongation) and 4000 GDDsim (between harvest/BBCH 99 and the DOYs corresponding to germination/BBCH 0 of a new seeding of winter wheat). When inspecting the results of extreme value analysis, it was discovered that the distribution within individual patterns of maxima and minima is larger, when compared to the compactness of break points' distribution. In regard to maxima (see Appendix A: Figure A2), VV and VH coherence cover mainly stages around 250 GDDs and between 3000 and 4000 GDDs. h2a_alpha, h2a_entropy, and CR only display a relevant pattern between BBCH 30 and BBCH 50, covering the timespan between stem elongation and heading. Maxima of VV and VH backscatter intensities also cover the time around BBCH 87 (yellow ripening) and partially extend towards BBCH 99 (harvest). When inspecting the relevant minima (see Appendix A: Figure A4), the pattern of h2a_alpha, h2a_entropy, and CR is inverted by the pattern exhibited by VV and VH backscatter, except for the part between harvest and germination, which is covered by all five features. Distinct occurrences of minima in coherence signals were observed for the time between stem elongation and heading. Additionally, VH coherence depicted a larger number of year-specific patterns.

This exemplary display regarding the major signal changes and their relation to phenological development showcases the depth of the insights that this form of analysis

can provide. However, describing and discussing minute discrepancies and consistencies was deemed out of scope for this article. Instead, summary plots such as Figure 7 were created to illustrate systematic findings across all five years and three relative orbits. Here, it was shown that break point occurrences of sugar beet exhibit a constant closeness (according to the threshold defined in Section 2.4.3) to the targeted stages. Crop signatures of canola also produced relevant occurrences close to the targeted stages, except for 2020. Especially, the occurrences around the end of flowering remained comparatively constant. Wheat displayed more variety; here, close patterns across all years were only found for stem elongation (BBCH 30) and heading (BBCH 50). The development of potato was also fully captured in 2018. Some of these findings are replicated by corresponding GDD distribution. For each crop type, several value ranges (see Figure 7, GD.) were identified in addition to the ones covering the targeted BBCH stages. Signatures of canola generated break point occurrences around 1000 GDDs and 2700 GDDs. In potato, signatures of such occurrences were found around 1200 GDDs, 1700 GDDs, and 2200 GDDs. Sugar beet featured such occurrences between 1500 GDDs and 2000 GDDs. Wheat produced additional concentrations of break points between BBCH 30 and BBCH 50, as well as around 3000 GDDs and 4000 GDDs.

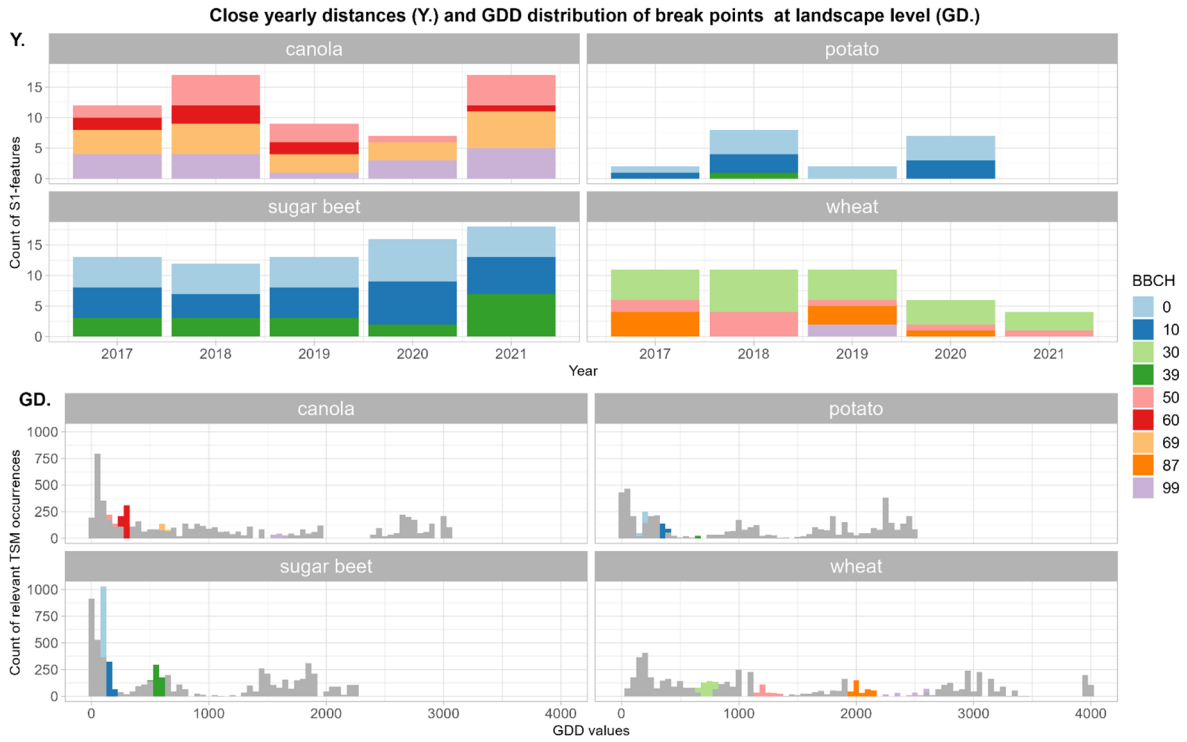

Figure 7. Year-wise count of S1 features producing break points (Y.) that closely track phenological stages by crop type and by their respective distribution of GDD values (GD.) at the landscape level which is overlaid by the GDD values of BBCH in situ observations (colored areas).

Maxima (see Figure A4) display a partially similar behavior (Y.), but canola, for example, produced mostly relevant occurrences around inflorescence (BBCH 50). All BBCH stages of sugar beet are represented by maxima, and yet canopy closure (BBCH 39) exhibits the largest S1 feature count. Stem elongation (BBCH 30), heading (BBCH 50), and yellow ripening (BBCH 87) of wheat exhibit maxima in four out of five years. Potato, in contrast, did not produce consistently close maxima to any BBCH stage. The GDD distribution (GD.) of canola also features similar ranges to break points around 700 GDDs and between 2700 and 3000 GDDs.

3.2. Tracking Reliability and Systematic Offsets

Since the corresponding DOY and GDD values of all TSM occurrences were subtracted from the corresponding values of the in situ observations and these differences aggregated over the entire observation period by mean and standard deviation, we were able to discern systematic and nonsystematic offsets by the thresholds mentioned in Section 2.4.3. The offsets of orbit and S1 feature that were deemed systematic by the threshold approach are displayed in Figure 6 by their mean deviation (*x*-axis) and their variance over time (standard deviation; *y*-axis). Furthermore, the results were separated by crop type and observed BBCH stage.

Figure 8 also illustrates systematic shifts related to orbit geometry. Such clear distinctions were found for inflorescence (BBCH 50) and end of flowering (BBCH 69) of canola, and harvest of wheat (BBCH 99), as well as for all three stages of potato. Clear preferences by S1 feature were discovered for yellow ripening of wheat (BBCH 87) as well as end of flowering of canola (BBCH 69).

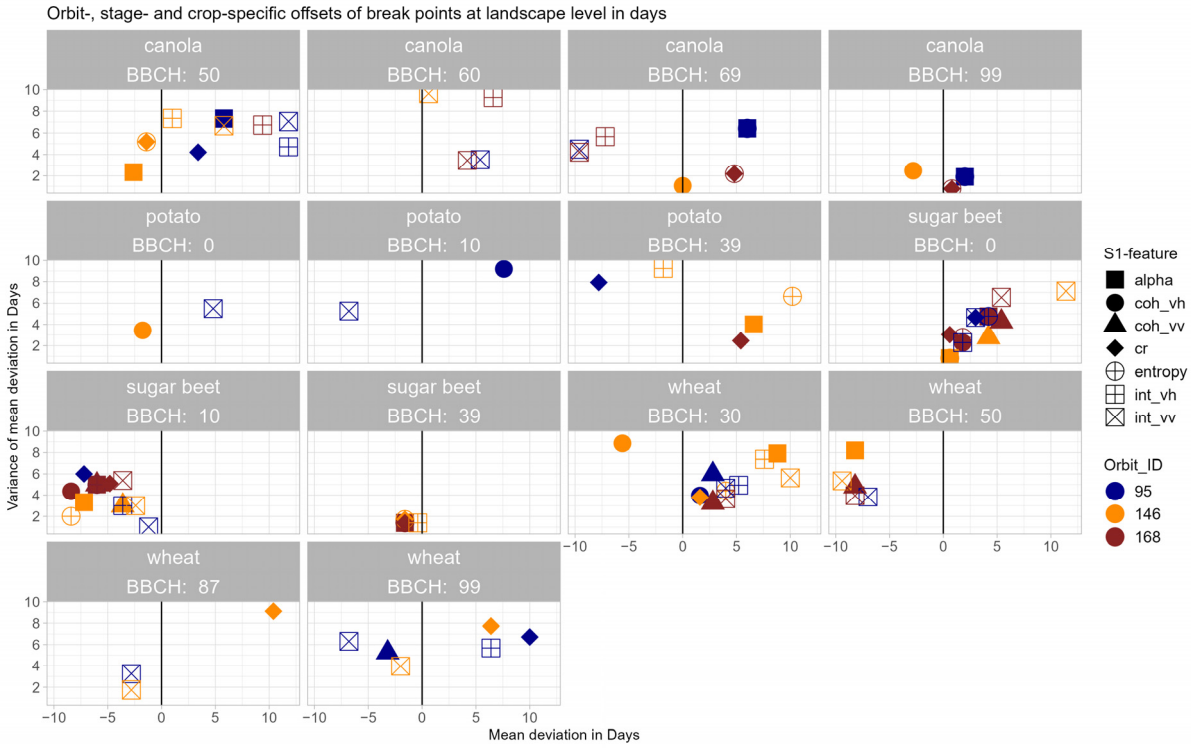

Figure 8. Orbit, stage, and crop-specific offsets of break points at landscape level in days, displaying their mean deviation from in situ observations and temporal variance (standard deviation) by crop type and BBCH stage, containing only tracked events that were labeled reliable by the threshold approach.

While Figure 8 depicts the entire set of S1 features that produced break point occurrences of reliable offset and variance in accordance with the threshold approach described in Section 2.4.3, Tables 4 and 5 list S1 features and their respective orbits that exhibited comparatively low variances and offsets for their targeted BBCH stage. For wheat, mostly intensity and coherence derived from orbits 95 and 146 were listed across all stages. With regard to canola, the majority of stages was closely tracked by a combination of intensity, alpha, and entropy, except for VH coherence at the end of flowering (BBCH 69). Sugar beet and potato, on the other hand, produced break point occurrences in all S1 features. In the case of sugar beet, VH coherence and intensity as well as alpha and entropy cover emergence (BBCH 0), whereas leaf development (BBCH 10) was closely tracked by VV intensity and coherence. Canopy closure (BBCH 39) featured occurrences by alpha, entropy, CR, and VH intensity.

Table 4. S1 features and their respective relative orbits producing reliable and comparatively close break point occurrences for wheat and canola.

Winter Wheat			Canola		
BBCH Stage	**S1 Feature**	**Orbit**	***BBCH Stage***	**S1 Feature**	**Orbit**
30	intensity_cr	146	***50***	h2a_alpha	146
	coherence_vh	95		intensity_cr	95
	coherence_vv	95		intensity_vh	146
	coherence_vv	168	***60***	intensity_vv	95
	intensity_vv	95		intensity_vv	168
50	intensity_vv	95	***69***	h2a_entropy	168
87	intensity_vv	95		intensity_cr	168
				coherence_vh	146
	intensity_vv	146	***99***	coherence_vh	146
99	coherence_vv	95		h2a_alpha	95
	intensity_vv	146		h2a_entropy	95
				h2a_entropy	168
				intensity_cr	168

Table 5. S1 features and their respective relative orbits producing reliable and comparatively close break point occurrences for sugar beet and potato.

Potato			Sugar Beet		
BBCH Stage	**S1 Feature**	**Orbit**	***BBCH Stage***	**S1 Feature**	**Orbit**
0	coherence_vh	146	**0**	coherence_vh	146
10	intensity_vv	95		coherence_vh	168
39	intensity_cr	168		h2a_alpha	146
	h2a_alpha	146		h2a_entropy	146
				intensity_vh	95
			10	intensity_vv	95
				intensity_vv	146
				coherence_vv	146
			39	h2a_alpha	168
				h2a_entropy	146
				h2a_entropy	168
				intensity_cr	146
				intensity_cr	168
				intensity_vh	146

As the same analysis was conducted for maxima and minima, it is evident (comparing Figures 8 and 9) that maxima track fewer phenological events. In the case of maxima, some sort of clustering for each relative orbit was observed for emergence (BBCH 0) of sugar beet as well as stem elongation (BBCH 30) and heading (BBCH 50). In parallel to the analysis of break points, the maxima of comparatively small mean deviation and variance are listed in Tables 6 and 7. Maxima in relation to wheat were found for stem elongation (BBCH 30) and yellow ripening (BBCH 87). The former was closely tracked by CR, alpha, and entropy derived from orbit 146, and the latter by VH intensity from orbits 168 and 95. Maxima in canola signatures were only found close to inflorescence (BBCH 50). These could be produced by alpha, entropy, and CR. Signatures of potatoes exhibited relevant occurrences of maxima in three stages: emergence (BBCH 0) was tracked by VH coherence from orbit 146, leaf development by VV intensity from orbit 95, and canopy closure (BBCH 39) could be traced by CR (orbit 168) and alpha (orbit 146). Sugar beet displayed also a stage-specific selection of S1 features. Maxima close to emergence (BBCH) were found in signatures of VH coherence of orbits 146 and 168, alpha and entropy of orbit 146, and VH intensity of orbit 95. Leaf development (BBCH) was tracked by VV intensity from orbit 146 and 95 as well as VV coherence of orbit 146. Canopy closure (BBCH) produced temporally close maxima in signatures of entropy, alpha, CR, and VH intensity from orbits 146 and 168.

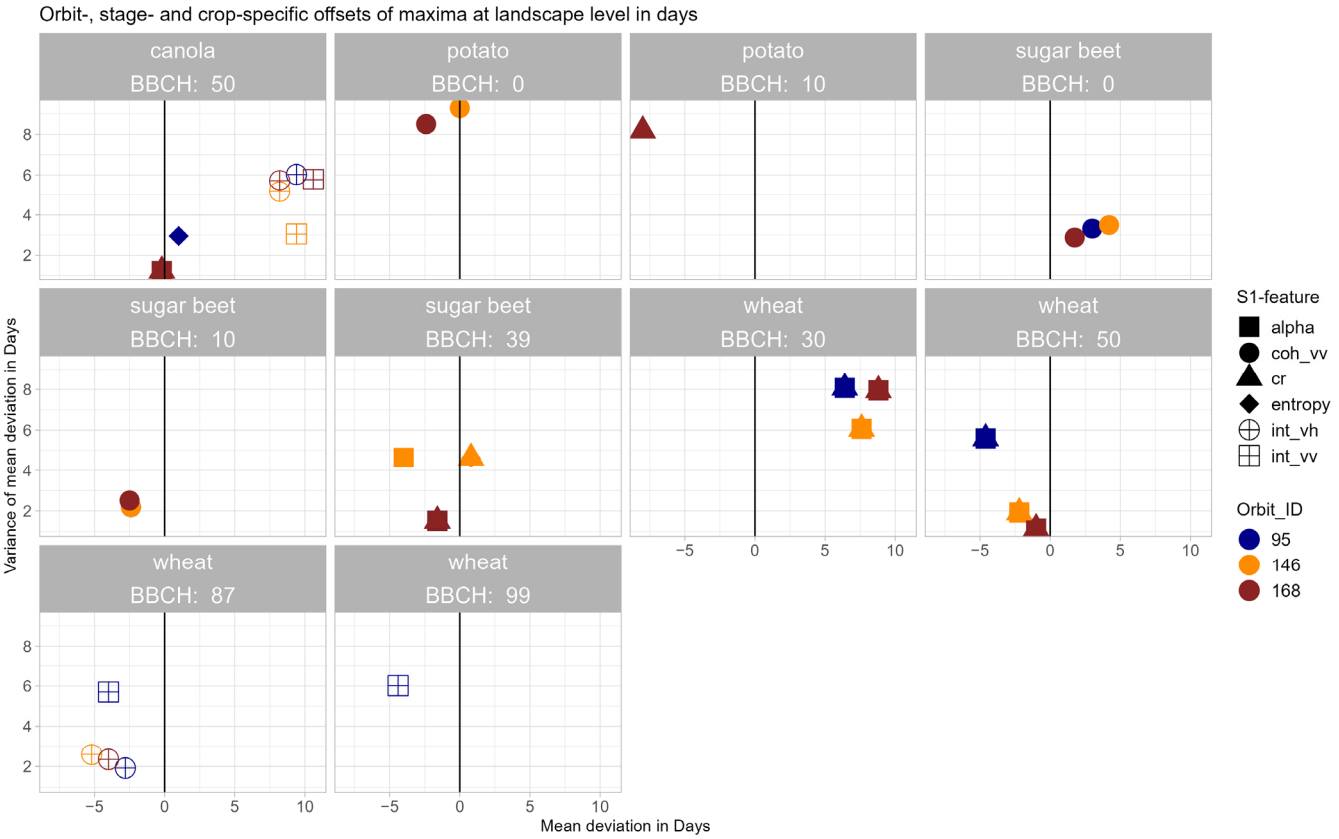

Figure 9. Orbit, stage, and crop-specific offsets of maxima at landscape level in days, displaying their mean deviation from in situ observations and temporal variance (standard deviation) by crop type and BBCH stage, containing only tracked events that were labeled reliable by the threshold approach.

Table 6. S1 features and their respective relative orbits producing reliable and comparatively close maxima occurrences for wheat and canola according to their mean offset and variance over the entire observation period.

Wheat			Canola		
BBCH Stage	**S1 Feature**	**Orbit**	***BBCH Stage***	**S1 Feature**	**Orbit**
30	intensity_cr	146	***50***	h2a_alpha	95
	h2a_entropy	146		h2a_alpha	146
	h2a_alpha	146		h2a_alpha	168
87	intensity_vh	168		h2a_entropy	95
	intensity_vh	95		h2a_entropy	146
				h2a_entropy	168
				intensity_cr	95
				intensity_cr	146
				intensity_cr	168

The investigation into relevant occurrences of minima yielded the following insights (illustrated by Figure 10) with regard to the trackability of the targeted stages: In terms of mean deviation and variance, clear separations by orbit were found for inflorescence (BBCH 50) of canola, harvest (BBCH 99) of wheat, and, to a certain degree, for leaf development (BBCH 10) of sugar beet. Similar to the results of maxima, the number of phenological stages that were labeled as reliably trackable is less in comparison to break points.

Table 7. S1 features and their respective relative orbits producing reliable and comparatively close maxima occurrences for potato and sugar beet.

Potato			Sugar Beet		
BBCH Stage	**S1 Feature**	**Orbit**	**BBCH Stage**	**S1 Feature**	**Orbit**
0	coherence_vh	146	0	coherence_vh	146
10	intensity_vv	95		coherence_vh	168
39	intensity_cr	168		h2a_alpha	146
	h2a_alpha	146		h2a_entropy	146
				intensity_vh	95
			10	intensity_vv	95
				intensity_vv	146
				coherence_vv	146
			39	h2a_alpha	168
				h2a_entropy	146
				h2a_entropy	168
				intensity_cr	146
				intensity_cr	168
				intensity_vh	146

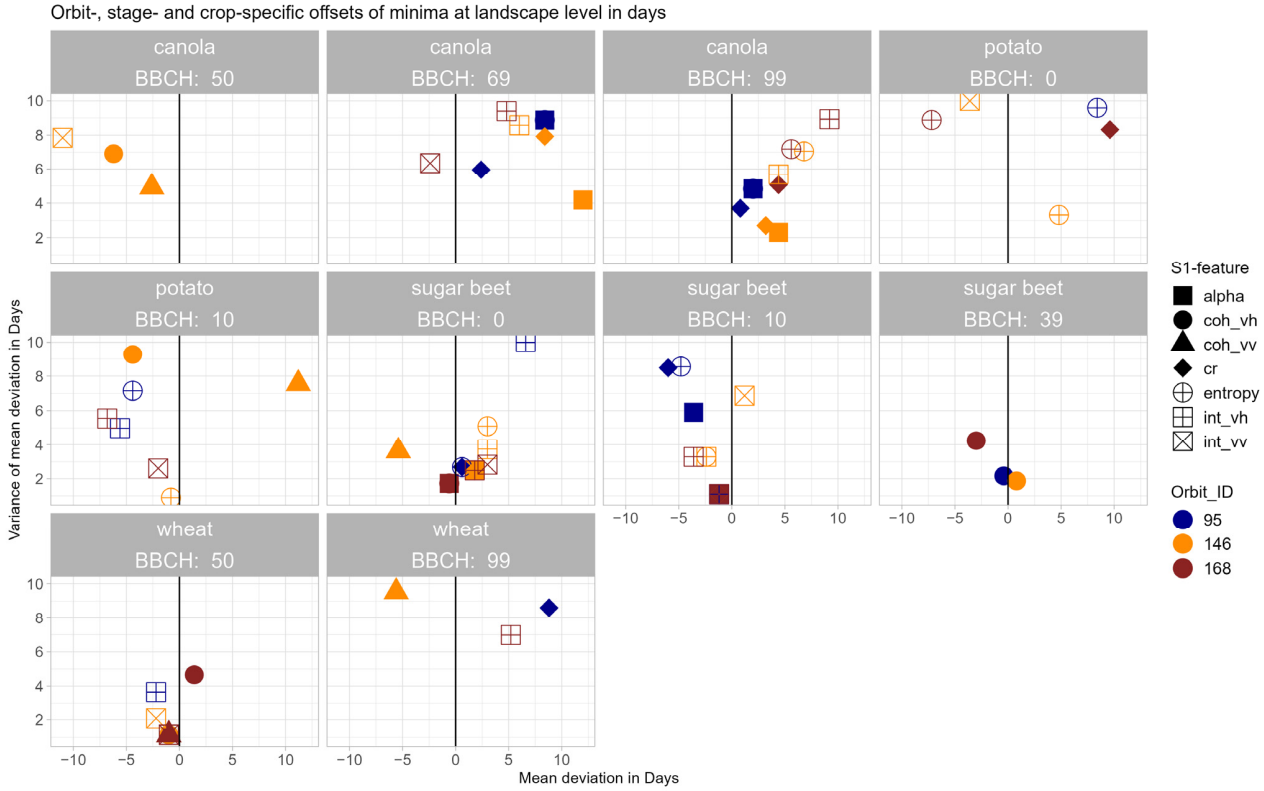

Figure 10. Orbit, stage, and crop-specific offsets of minima at landscape level in days, displaying their mean deviation from in situ observations and temporal variance (standard deviation) by crop type and BBCH stage, containing only tracked events that were labeled reliable by the threshold approach.

Minima of comparatively close distance and low variance are listed in Tables 8 and 9. For heading of wheat, VV and VH coherence of all orbits are the dominant S1 features, whereas harvest (BBCH 99) is only covered by VH intensity from orbit 168. For canola, inflorescence (BBCH 50) was tracked by VV coherence (orbit 146) and intensity (orbit 168), as well as CR (orbit 95). End of flowering (BBCH 69) was covered by alpha and entropy from orbit 95 and the harvest (BBCH 99) by CR being derived from orbits 95 and 146. Occurrences of relevant minima were found in potato signatures of entropy for emergence and leaf development (BBCH 0 and 10). Regarding the development of sugar beet, alpha,

entropy, and CR were close to emergence (BBCH 0) mostly in all orbits. Leaf development could be tracked by minima of VV and VH intensity as well as CR via orbits 146 and 168. Minima in VH coherence were detected close to canopy closure (BBCH 39).

Table 8. S1 features and their respective relative orbits producing reliable and comparatively close maxima occurrences for wheat and canola.

Wheat			Canola		
BBCH Stage	**S1 Feature**	**Orbit**	*BBCH Stage*	**S1 Feature**	**Orbit**
50	coherence_vh	95	***50***	coherence_vv	146
	coherence_vh	146		intensity_vv	168
	coherence_vh	168		intensity_cr	95
	coherence_vv	95	***69***	h2a_alpha	95
	coherence_vv	146		h2a_entropy	95
	coherence_vv	168	***99***	intensity_cr	95
	intensity_vv	168		intensity_cr	146
99	intensity_vh	168			

Table 9. S1 features and their respective relative orbits producing reliable and comparatively close maxima occurrences for sugar beet and potato.

Potato			Sugar Beet		
BBCH Stage	**S1 Feature**	**Orbit**	*BBCH Stage*	**S1 Feature**	**Orbit**
0	h2a_entropy	146	***0***	h2a_alpha	95
10	h2a_entropy	146		h2a_alpha	146
	intensity_vv	168		h2a_alpha	168
				h2a_entropy	95
				h2a_entropy	146
				h2a_entropy	168
				intensity_cr	95
				intensity_cr	146
				intensity_cr	168
				intensity_vh	168
			10	intensity_cr	146
				intensity_cr	168
				intensity_vh	95
				intensity_vh	146
				intensity_vh	168
				intensity_vv	146
				intensity_vv	168
				h2a_alpha	168
				h2a_entropy	168
			39	coherence_vh	95
				coherence_vh	146

4. Discussion

4.1. Discussing Patterns of Major Signal Change

The results of the investigation into patterns of major signal changes revealed and reaffirmed serveral key aspects of SAR-based time series analyses. This is, to the extent the authors are aware of, the first systematic study to analyze the relation between C-Band SAR signals and phenological development of crops in an investigative approach encompassing three relative orbits, five years, seven S1 features, two types of TSMs, and four different crop types, as well as their BBCH stages. In addition to that, a novel approach of detecting windows of phenologically induced change was applied by stacking time series of different smoothing intensity to estimate the density of TSM occurrences.

Because the coverage of the targeted BBCH stages also implies insights into reliability and offset, this is discussed in detail in Section 4.2. But apart from the targeted stages,

the potential to cover additional time windows was demonstrated. Furthermore, the integration of a GDD baseline provided a second temporal coordinate to evaluate the tracking reliability of such events. Judging by their DOY values, the example of wheat signatures contains likely freezing and thawing events around DOY 55 to 67 as well as the transition into the catch crop stage alongside the reemergence of subsequent winter crops. Similar observations were made for the other three crop types as well. Potato and sugar beet also displayed additional TSM occurrences during their development up to the likely period of harvesting. Such patterns were better discernable for break points as extrema exhibited larger time windows. This reiterates the need to filter phenologically nonrelevant extrema [30] or to limit the tracking to specific stages such as flowering of canola [29].

By conducting this analysis in a multiannual framework encompassing various agro-meteorological conditions, phenological events that shape a crop-specific time series regardless of weather conditions and signal processing were revealed in relation to their viewing geometry. Hereby, highly active and inactive periods in terms of signal change were placed into the context of plant lifecycles. In addition, this demonstrated the potential to reveal parts of said plant lifecycles that are reliably traceable and not covered by the DWD monitoring framework. This would suggest an added value of Earth-observation-based monitoring setups for phenological monitoring, because data gaps would be filled. The multiannual framework also highlighted the clear borders of the calibration periods required for such an approach. The first local extreme values, which are not at the start and end of the time series, were found as early as 20 to 25 days into the yearly observation period break points provided only insights into yearly developments between DOY 50 and 300. This quantification of the calibration periods constitutes a contribution to the discussion of information availability in time series [21] within the context of civil years.

4.2. Discussing Reliability and Systematic Offsets

As this study uses the DWD statistics on a federal level, the fact that major signal changes are not necessarily linked to the onset of that particular micro stadium cannot be fully discarded. Moreover, the results of the temporal thresholding (see Figures 8–10) showed that signal changes were not necessarily related to the onset of BBCH stages represented by in situ data. It is considered likely that adjacent micro stadia, in the case of wheat and stem elongation BBCH 31 or 35, rather than 30 were depicted. This corroborates the findings by [18,22].

Nevertheless, crop- and stage-specific sets of S1 features that produced close TSM occurrences were identified. Overall, more stages could be closely tracked by break points rather than extrema. This is most likely related to the wider range of uncertainty of extrema and their respective time windows of phenological changes (see Figures A2 and A4).

With regard to break points, the targeted stages of winter wheat were best tracked by VV intensity and coherence of orbits 95 and 146, reflecting the plant's vertical structure. The listing of coherence for stem elongation and harvest (BBCH 30 and 99) demonstrated the features sensitivity to significant changes in volume of biomass [17,18]. The absence of orbit 168 suggests that tracking wheat phenology might be susceptible to moisture content when using moderate incidence angles. Otherwise, a clear preference of steeper incidence angles was only found at heading (BBCH 50). Such a clear overall preference in viewing geometry was not found for canola. Only stage-specific preferences for the start and end of flowering (BBCH 60 and 69) were found regarding moderate incidence angles. Here, h2a_entropy and h2a_alpha, as well as intensity_cr, featured the closest occurrences of break points. The preference of h2a and CR is most likely related to the complex structure of canola plants, as they reflect a change in dominant scattering type. Furthermore, VV intensity being the favorable S1 feature for tracking onset of flowering (BBCH 60) fits the increased sensitivity of VV polarization to superficial changes of the canopy [29,31]. Some of these findings are also replicable for sugar beet signatures. First of all, significant changes at the land surface such as emergence (BBCH 0) or leaf development were captured by coherence. Secondly, h2a and intensity_cr could be linked to canopy closure, which coincides with the time when

the plant's physiognomy is comparatively complex. However, sugar beet favors incidence angles of moderate range, which is most likely related to its low height in comparison to wheat or canola. The break points within signatures of potato exhibit a similar behavior, similar to wheat orbit 95, and to some degree, 146 was favored. A tendency towards steeper incidence angles was only found at leaf development (BBCH 10).

Results of the extreme value analyses overlap with these observations; however, there are some notable differences. Heading (BBCH 50) of wheat produced local maxima in coherence signatures, suggesting that the crop volume was stable enough to increase the temporal correlation above noise level, regardless of the incidence angle. This particular occurrence has not been observed by comparable studies [17,19]. A similar observation was made for inflorescence (BBCH 50) of canola in VV coherence; however, this was only related to moderate incidence angles. Another, more evident difference was discovered for sugar beet. Here, extreme values did not show any preference of orbit, but displayed a similar performance across all viewing geometries. This is most likely related to the aforementioned finding, that extrema can be produced over larger time windows.

While unequivocal indications for a complementary tracking potential of different S1 features was only found for BBCH 69 of canola and BBCH 0 of potatoes, the increased number of listings around strong changes in biomass (harvest, stem elongation) or disturbances of the soil agree with findings of previous studies [14,17,18,59], that InSAR coherence increases the trackability of certain phenological stages. On the other hand, h2a_entropy and h2a_alpha seem to provide less added value and can be replaced by intensity, especially CR, in a dual-pol C-Band framework.

Considering the results of break points and extrema in relation to time of overpass, moisture content within the canopy is rated as a secondary effect. But because the results of the orbit-wise comparisons of wheat, canola, and sugar beet differ mostly by comparatively small margins, it is also likely that the increased closeness to in situ observations originates from a favorable revisiting schedule that is temporally closer to the onsite phenological developments, especially because this study uses the DWD statistics at the level of federal state. On top of these issues, the analysis of potato signatures was additionally hampered by the comparatively small number of fields (twelve fields of potato vs. 500 fields of wheat), which increases the impact of outliers on a generalized pattern at the landscape level. Moreover, fields of potato in Demmin are characterized by rather heterogeneous conditions due to the cultivation of different sorts of potato as well as the application of sprinkle irrigation. Therefore, the statements made about phenological developments of potatoes are considered less robust and serve more as a first impression.

Assessing another anticipated shortcoming, the references of DOYs corresponding to BBCH 0 and BBCH 10 for winter crops as general points of orientation within phenological progress of the civil year worked well in the chapter on major signal changes, and the deliberate focus on the civil year ensured the comparability between the progress of all four crop types. The GDDsim baseline is also affected by this decision, resulting in larger counts of relevant GDDsim accumulations at the start of this season. Therefore, further studies on that subject should account for this aspect. Nevertheless, the GDDsim baseline enabled an initial quantification of relevant TSM patterns which were not covered by the in situ observations. In addition, each of the TSM occurrences, as well as the in situ observations, are now associated with a GDDsim value; thus, progress towards a certain BBCH stage or the next occurrence of relevant TSM patterns is easily quantifiable in subsequent studies on this subject.

Needless to say, this study relies on the availability of information on crop types and field boundaries, but these are also issues that the Earth observation community has investigated. Therefore, there are solutions to overcome the lack of information on field boundaries [60,61] or crop types [62].

4.3. Outlook

This successful investigation into phenologically induced pattern of S1 time series at the landscape level opens up two major directions for future research.

On the one side, an allocation of field-level developments within the general pattern of the landscape is possible. This information can be used to check whether a field is early or late in its phenological development when compared to the general trend at landscape level. This would result in a more spatially explicit information than the interpolated 1 km grid of phenological progression provided by DWD. Additionally, a strong deviation from the landscape level patterns may serve as an indicator for field-specific crop stress such as lodging or pest infestation. On the other side, an archive of recorded phenological events and their relation to a growing degree baseline has been established. As pointed out by Harfenmeister et al. [22], and as was made evident during this study, back-looking approaches such as break point and extreme value analyses are not easily converted to a near-real-time application due to their calibration phases that may stretch across multiple weeks. However, the satellite- and GDDsim-based records of said archive could be leveraged in a comparative scenario analysis to assess the performance of an ongoing season. This could be accomplished by a comparison between its S1-based time series and the accumulation of GDDs with the successfully tracked phenological development of past seasons. Furthermore, by including weather forecasts, even an outlook may be provided, as the distance to the next phenological event on record also contains a respective GDDsim value. Hence, the projected GDD accumulation from the weather forecast can be employed to estimate the phenological progress of the ongoing season in comparison to the seasons on record.

Finally, the transferability of the approach in space and time, especially with regard to the added value of a GDD baseline, as well as the inclusion of spectral information are deemed sensible objectives for further investigation.

5. Conclusions

This study produced comprehensive insights into how phenology of wheat, canola, sugar beet, and potato shape their respective S1 signatures in different weather conditions, their inherent viewing geometry, and regardless of how strongly the time series is smoothed or processed otherwise. This leads to the following conclusions about TSM analyses:

(i) Break points constitute a better tool for entire-season monitoring, while extrema are mainly suitable for specific stages, because of the great variations detected in patterns of extreme values.
(ii) It is therefore crucial to optimize time signal processing for targeted stages or focus on specific parts of the crop lifecycle when employing extreme value analysis.
(iii) This study demonstrates its suitability for entire-season coverage of the crop lifecycle, as a single optimized smoothing of time series will inevitably hamper the capabilities of a monitoring framework to detect certain macro or micro stadia of crop development.

This approach also generated a designation of reliable S1 features by crop type and relative orbit for the area of Demmin. An overall great suitability of backscatter intensities was confirmed, and orbits favorable for tracking specific crop types were discovered. The most prominent findings are as follows:

(iv) A moderate range of incidence angles between 31°and 41° (orbit 146 and 168) is better suited than a range between 41° and 45° (orbit 95) for tracking crop phenology of sugar beet and wheat, whereas potatoes favor steeper angles. There are, however, BBCH- and S1-feature-specific exceptions to these tendencies.
(v) Relevant signal changes often corresponded to surrounding micro stadia of the onset of a macro stadium, instead of the onset itself.
(vi) With respect to times of overpass, only wheat displayed visible tendencies to favor the late afternoon.
(vii) VV and VH intensity outperformed the other features in terms of overall reliability. There are, however, specific combinations of crop type and BBCH stadia, where a complementary dataset of PolSAR and coherence provides added value and increased robustness.

By adding an artificial GDD baseline, the quantification of progress towards targeted stages by their thermal growth potential was achieved. This enables the relation of the established patterns at the landscape level to phenological developments of individual fields, because every TSM and BBCH stage at the landscape and at field levels were assigned a corresponding GDD value. This, in turn, sets up objectives of further studies such as the analysis of spatial patterns in phenological developments within the landscape and the potential to highlight field-specific anomalies in the crop lifecycle.

Author Contributions: Conceptualization, J.L. and T.U.; methodology, J.L.; software, J.L. and S.H.; validation, J.L.; formal analysis, J.L.; investigation, J.L.; resources, M.T. and C.C.; data curation, J.L. and S.H.; writing—original draft preparation, J.L.; writing—review and editing, J.L., I.O., M.T., T.U. and C.C.; visualization, J.L.; supervision, T.U. and C.C.; project administration, J.L., I.O., M.T. and C.C.; funding acquisition, M.T. and C.C. All authors have read and agreed to the published version of the manuscript.

Funding: This research was funded by German Aerospace Center (PhenoSAR: Demmin: FKZ: 0067286236), Martin-Luther-University of Halle-Wittenberg, as well as the German Ministry of Agriculture via the project of AgriSens Demmin 4.0 (FKZ: 28DE114E18).

Data Availability Statement: Data and software will be made available upon request. The InVeKoS data are excluded from this statement, because they were obtained based on an agreement that does not allow sharing with third parties.

Acknowledgments: We would like to thank ESA for providing open access to Sentinel-1 data as well as our project partners for supplying the data on field boundaries and crop types.

Conflicts of Interest: The authors declare no conflicts of interest.

Appendix A

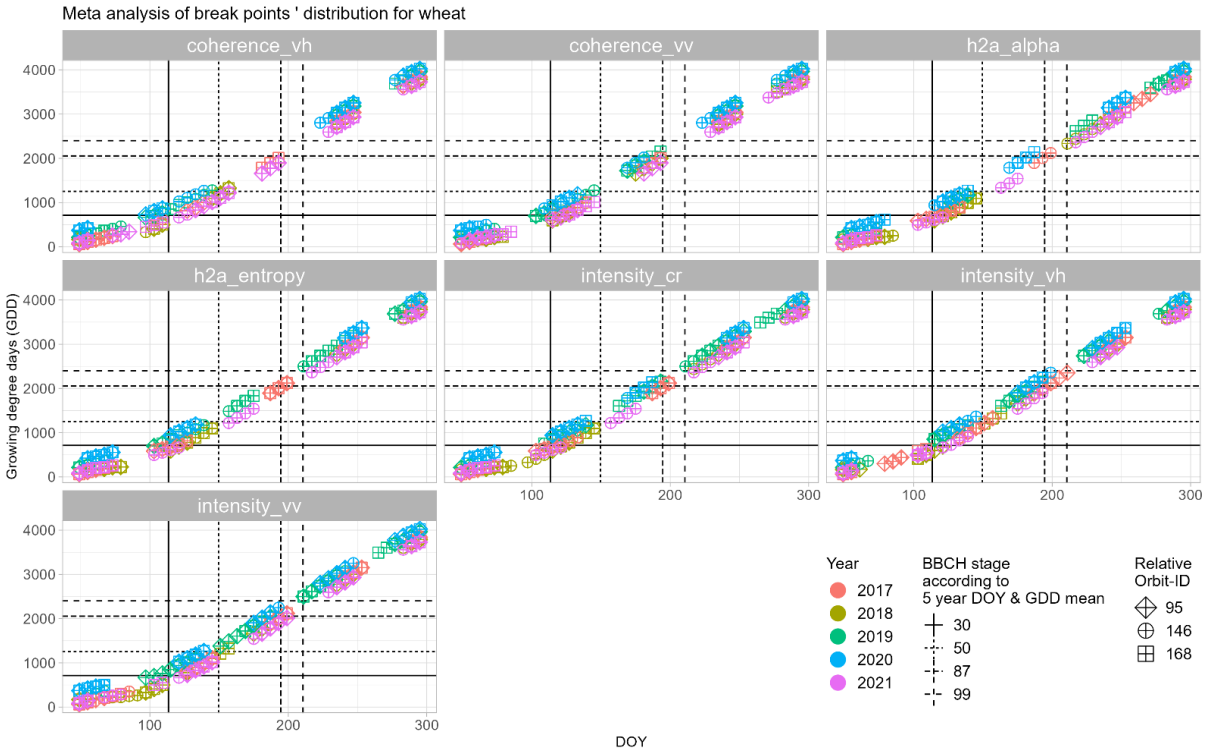

Figure A1. Orbit-specific patterns of major signal changes at landscape level tracked by break points according to day of year (DOY; *x*-axis) and artificial growing degree day (GDDsim) values (*y*-axis) in relation to the corresponding five-year mean GDD value of BBCH stadia observed by DWD at landscape level from 2017 to 2021. Exemplary illustration for fields of winter wheat.

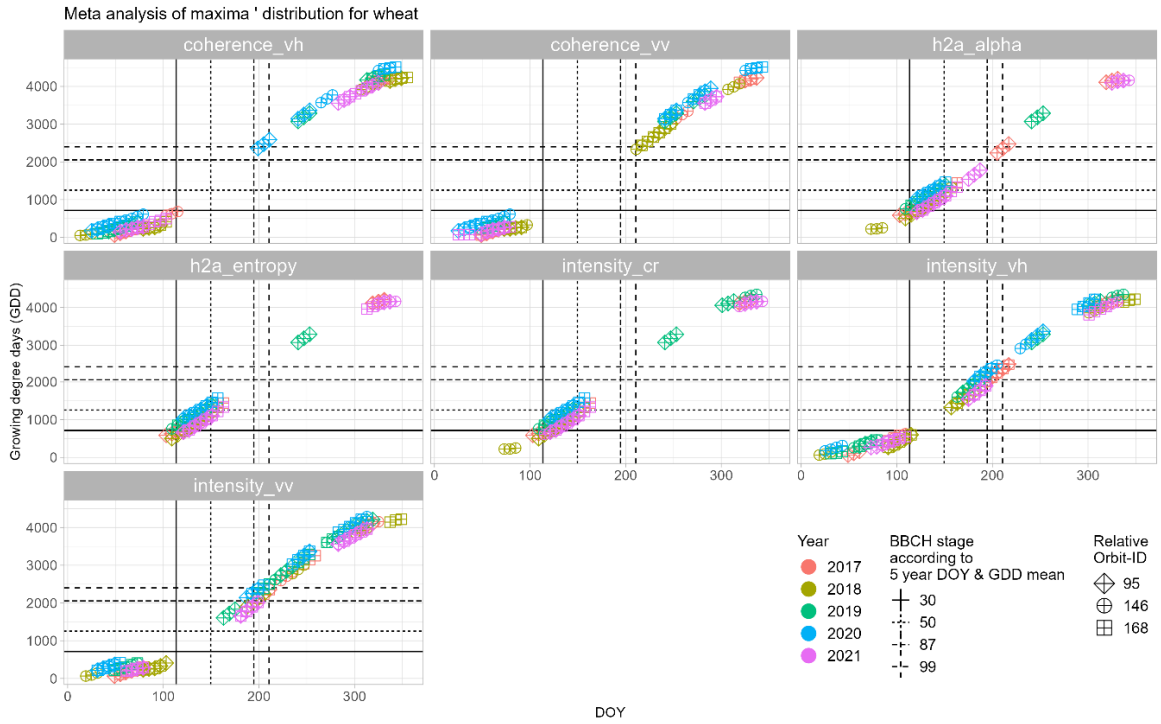

Figure A2. Orbit-specific patterns of major signal changes by maxima by day of year (DOY; *x*-axis) and growing degree day (GDDsim) values (*y*-axis) in relation to the corresponding five-year mean GDDsim value of BBCH stadia observed by DWD at landscape level from 2017 to 2021. Exemplary illustration for fields of winter wheat.

Figure A3. Year-wise count of S1 features producing maxima (Y.) that closely track phenological stages by crop type and by their respective distribution of GDD values (GD.)at the landscape level which is overlaid by the GDD values of BBCH in situ observations (colored areas).

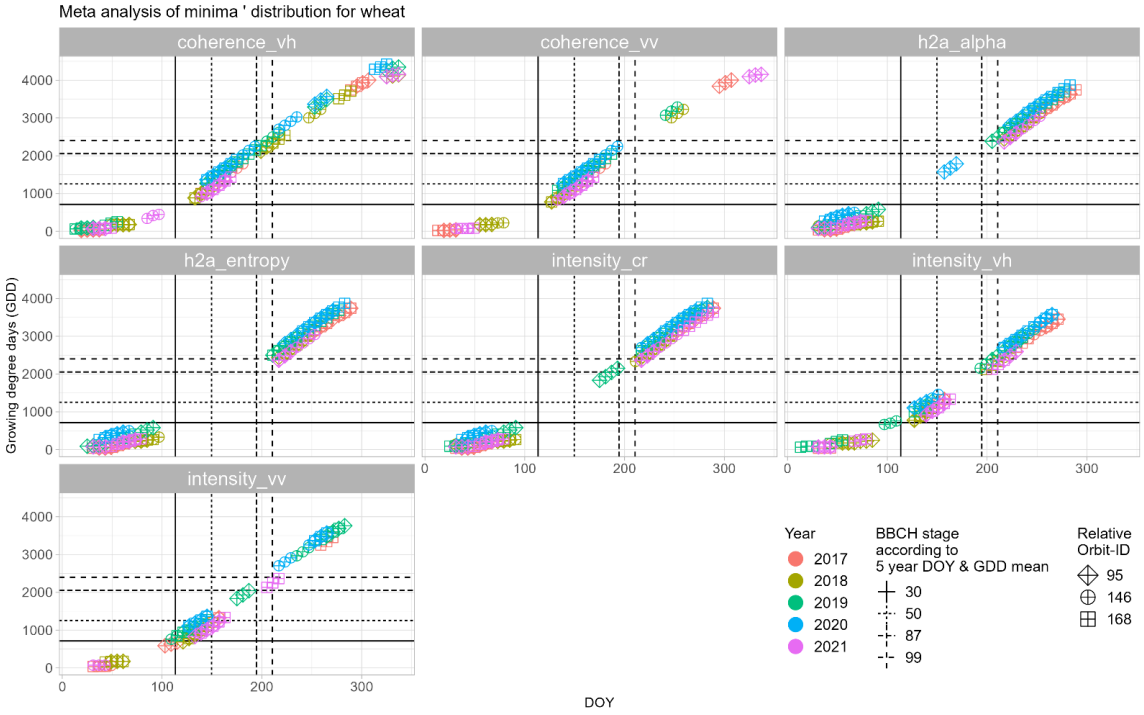

Figure A4. Orbit-specific patterns of major signal changes by minima by day of year (DOY; *x*-axis) and growing degree day (GDDsim) values (*y*-axis) in relation to the corresponding five-year mean GDDsim value of BBCH stadia observed by DWD at landscape level from 2017 to 2021. Exemplary illustration for fields of winter wheat.

Figure A5. Year-wise count of S1 features producing minima (Y.) that closely track phenological stages by crop type and by their respective distribution of GDD values (GD.)at the landscape level which is overlaid by the GDD values of BBCH in situ observations (colored areas).

References

1. Whitcraft, A.K.; Becker-Reshef, I.; Justice, C.O.; Gifford, L.; Kavvada, A.; Jarvis, I. No Pixel Left behind: Toward Integrating Earth Observations for Agriculture into the United Nations Sustainable Development Goals Framework. *Remote Sens. Environ.* **2019**, *235*, 111470. [CrossRef]
2. Gilliams, S.; Whitcraft, A.; Kommareddy, I.; Haynes, K.; Jarvis, I. EAV Home | AgVariables. Available online: https://agvariables.org/ (accessed on 29 November 2023).
3. Gao, F.; Anderson, M.C.; Zhang, X.; Yang, Z.; Alfieri, J.G.; Kustas, W.P.; Mueller, R.; Johnson, D.M.; Prueger, J.H. Toward Mapping Crop Progress at Field Scales through Fusion of Landsat and MODIS Imagery. *Remote Sens. Environ.* **2017**, *188*, 9–25. [CrossRef]
4. Stathers, T.; Lamboll, R.; Mvumi, B.M. Postharvest Agriculture in Changing Climates: Its Importance to African Smallholder Farmers. *Food Secur.* **2013**, *5*, 361–392. [CrossRef]
5. Sakamoto, T.; Gitelson, A.A.; Arkebauer, T.J. MODIS-Based Corn Grain Yield Estimation Model Incorporating Crop Phenology Information. *Remote Sens. Environ.* **2013**, *131*, 215–231. [CrossRef]
6. Baghdadi, N.; Boyer, N.; Todoroff, P.; El Hajj, M.; Bégué, A. Potential of SAR Sensors TerraSAR-X, ASAR/ENVISAT and PALSAR/ALOS for Monitoring Sugarcane Crops on Reunion Island. *Remote Sens. Environ.* **2009**, *113*, 1724–1738. [CrossRef]
7. Shorachi, M.; Kumar, V.; Steele-Dunne, S.C. Sentinel-1 SAR Backscatter Response to Agricultural Drought in The Netherlands. *Remote Sens.* **2022**, *14*, 2435. [CrossRef]
8. Steele-Dunne, S.C.; McNairn, H.; Monsivais-Huertero, A.; Judge, J.; Liu, P.W.; Papathanassiou, K. Radar Remote Sensing of Agricultural Canopies. *IEEE J. Sel. Top. Appl. Earth Obs. Remote Sens.* **2017**, *10*, 2249–2273. [CrossRef]
9. Nasrallah, A.; Baghdadi, N.; El Hajj, M.; Darwish, T.; Belhouchette, H.; Faour, G.; Darwich, S.; Mhawej, M. Sentinel-1 Data for Winter Wheat Phenology Monitoring and Mapping. *Remote Sens.* **2019**, *11*, 2228. [CrossRef]
10. Atzberger, C. Advances in Remote Sensing of Agriculture: Context Description, Existing Operational Monitoring Systems and Major Information Needs. *Remote Sens.* **2013**, *5*, 949–981. [CrossRef]
11. Vreugdenhil, M.; Wagner, W.; Bauer-Marschallinger, B.; Pfeil, I.; Teubner, I.; Rüdiger, C.; Strauss, P. Sensitivity of Sentinel-1 Backscatter to Vegetation Dynamics: An Austrian Case Study. *Remote Sens.* **2018**, *10*, 1396. [CrossRef]
12. Pasternak, M.; Pawłuszek-Filipiak, K. Evaluation of C and X-Band Synthetic Aperture Radar Derivatives for Tracking Crop Phenological Development. *Remote Sens.* **2023**, *15*, 4996. [CrossRef]
13. Mercier, A.; Betbeder, J.; Baudry, J.; Le Roux, V.; Spicher, F.; Lacoux, J.; Roger, D.; Hubert-Moy, L. Evaluation of Sentinel-1 & 2 Time Series for Predicting Wheat and Rapeseed Phenological Stages. *ISPRS J. Photogramm. Remote Sens.* **2020**, *163*, 231–256. [CrossRef]
14. Lobert, F.; Löw, J.; Schwieder, M.; Gocht, A.; Schlund, M.; Hostert, P.; Erasmi, S. A Deep Learning Approach for Deriving Winter Wheat Phenology from Optical and SAR Time Series at Field Level. *Remote Sens. Environ.* **2023**, *298*, 113800. [CrossRef]
15. McNairn, H.; Jiao, X.; Pacheco, A.; Sinha, A.; Tan, W.; Li, Y. Estimating Canola Phenology Using Synthetic Aperture Radar. *Remote Sens. Environ.* **2018**, *219*, 196–205. [CrossRef]
16. Canisius, F.; Shang, J.; Liu, J.; Huang, X.; Ma, B.; Jiao, X.; Geng, X.; Kovacs, J.M.; Walters, D. Tracking Crop Phenological Development Using Multi-Temporal Polarimetric Radarsat-2 Data. *Remote Sens. Environ.* **2018**, *210*, 508–518. [CrossRef]
17. Schlund, M.; Erasmi, S. Sentinel-1 Time Series Data for Monitoring the Phenology of Winter Wheat. *Remote Sens. Environ.* **2020**, *246*, 111814. [CrossRef]
18. Löw, J.; Ullmann, T.; Conrad, C. The Impact of Phenological Developments on Interferometric and Polarimetric Crop Signatures Derived from Sentinel-1: Examples from the DEMMIN Study Site (Germany). *Remote Sens.* **2021**, *13*, 2951. [CrossRef]
19. Khabbazan, S.; Vermunt, P.; Steele-Dunne, S.; Arntz, L.R.; Marinetti, C.; van der Valk, D.; Iannini, L.; Molijn, R.; Westerdijk, K.; van der Sande, C. Crop Monitoring Using Sentinel-1 Data: A Case Study from The Netherlands. *Remote Sens.* **2019**, *11*, 1887. [CrossRef]
20. Meier, U. *Growth Stages of Mono-and Dicotyledonous Plants. BBCH Monograph*, 2nd ed.; Meier, U., Ed.; Federal Biological Research Centre for Agriculture and Forestry: Berlin, Germany; Braunschweig, Germany, 2001.
21. Harfenmeister, K.; Itzerott, S.; Weltzien, C.; Spengler, D. Agricultural Monitoring Using Polarimetric Decomposition Parameters of Sentinel-1 Data. *Remote Sens.* **2021**, *13*, 575. [CrossRef]
22. Harfenmeister, K.; Itzerott, S.; Weltzien, C.; Spengler, D. Detecting Phenological Development of Winter Wheat and Winter Barley Using Time Series of Sentinel-1 and Sentinel-2. *Remote Sens.* **2021**, *13*, 5036. [CrossRef]
23. McMaster, G.S.; Wilhelm, W.W. Growing Degree-Days: One Equation, Two Interpretations. *Agric. For. Meteorol.* **1997**, *87*, 291–300. [CrossRef]
24. European Space Agency Mission Ends for Copernicus Sentinel-1B Satellite. Available online: https://www.copernicus.eu/en/news/news/mission-ends-copernicus-sentinel-1b-satellite (accessed on 8 April 2024).
25. Gorrab, A.; Ameline, M.; Albergel, C.; Baup, F. Use of Sentinel-1 Multi-Configuration and Multi-Temporal Series for Monitoring Parameters of Winter Wheat. *Remote Sens.* **2021**, *13*, 553. [CrossRef]
26. Arias, M.; Campo-Bescós, M.Á.; Álvarez-Mozos, J. On the Influence of Acquisition Geometry in Backscatter Time Series over Wheat. *Int. J. Appl. Earth Obs. Geoinf.* **2022**, *106*, 102671. [CrossRef]
27. Qadir, A.; Skakun, S.; Eun, J.; Prashnani, M.; Shumilo, L. Sentinel-1 Time Series Data for Sunflower (*Helianthus annuus*) Phenology Monitoring. *Remote Sens. Environ.* **2023**, *295*, 113689. [CrossRef]
28. Cai, Z.; Jönsson, P.; Jin, H.; Eklundh, L. Performance of Smoothing Methods for Reconstructing NDVI Time-Series and Estimating Vegetation Phenology from MODIS Data. *Remote Sens.* **2017**, *9*, 1271. [CrossRef]

29. d'Andrimont, R.; Taymans, M.; Lemoine, G.; Ceglar, A.; Yordanov, M.; van der Velde, M. Detecting Flowering Phenology in Oil Seed Rape Parcels with Sentinel-1 and -2 Time Series. *Remote Sens. Environ.* **2020**, *239*, 111660. [CrossRef] [PubMed]
30. Meroni, M.; d'Andrimont, R.; Vrieling, A.; Fasbender, D.; Lemoine, G.; Rembold, F.; Seguini, L.; Verhegghen, A. Comparing Land Surface Phenology of Major European Crops as Derived from SAR and Multispectral Data of Sentinel-1 and -2. *Remote Sens. Environ.* **2021**, *253*, 112232. [CrossRef] [PubMed]
31. Woodhouse, I.H. *Introduction to Microwave Remote Sensing*; CRC Press: Boca Raton, FL, USA, 2006.
32. Borg, E.; Fichtelmann, B.; Zabel, E.; Maasss, H. Test Site for Calibration and Validation of Remote Sensing Missions, Sensors, Data and Value Added Products. In Proceedings of the LANDSAT Ground Station Operators's Working Group# 38 (LGSOWG), Berlin, Germany, 28 September–5 October 2009.
33. Small, D. Flattening Gamma: Radiometric Terrain Correction for SAR Imagery. *IEEE Trans. Geosci. Remote Sens.* **2011**, *49*, 3081–3093. [CrossRef]
34. BaySTMELF. *Anleitung Zum Ausfüllen Des Flächen- Und Nutzungsnachweises (FNN) 2022*; Bayerisches Staatsministerium für Ernährung, Landwirtschaft, Forsten und Tourismus: Munich, Germany, 2022.
35. Kaspar, F.; Zimmermann, K.; Polte-Rudolf, C. An Overview of the Phenological Observation Network and the Phenological Database of Germany's National Meteorological Service (Deutscher Wetterdienst). *Adv. Sci. Res.* **2015**, *11*, 93–99. [CrossRef]
36. Ritchie, J.T.; Nesmith, D.S. Temperature and Crop Development. In *Modeling Plant and Soil Systems*; Wiley Blackwell: Hoboken, NJ, USA, 2015; pp. 5–29, ISBN 9780891182238.
37. Stinner, R.E.; Gutierrez, A.P.; Butler, G.D. An Algorithm for Temperature-Dependent Growth Rate Simulation. *Can. Entomol.* **1974**, *106*, 519–524. [CrossRef]
38. Zhou, G.; Wang, Q. A New Nonlinear Method for Calculating Growing Degree Days. *Sci. Rep.* **2018**, *8*, 10149. [CrossRef] [PubMed]
39. Haßelbusch, K.; Lucas-Mofat, A. *Rasterdaten Für Die Agrarmeteorologie: Vergleich Verschiedener Interpolationsverfahren Am Beispiel AgriSens Demmin 4.0*; Deutscher Wetterdienst: Braunschweig, Germany, 2021.
40. Killough, B. Overview of the Open Data Cube Initiative. In Proceedings of the International Geoscience and Remote Sensing Symposium (IGARSS), Valencia, Spain, 22–27 July 2018; Institute of Electrical and Electronics Engineers Inc.: Piscataway, NJ, USA, 2018; pp. 8629–8632.
41. Friedrich, C.; Löw, J.; Otte, I.; Hill, S.; Förtsch, S.; Schwalb-Willmann, J.; Gessner, U.; Schierghofer, C.; Truckenbrodt, S.; Schonert, E.; et al. A Multi-Talented Datacube: Integrating, Processing and Presenting Big Geodata for the Agricultural End User. In *Proceedings of the Informatik in der Land-, Forst und Ernährungswirtschaft. Fokus: Biodiversität Fördern Durch Digitale Landwirtschaft*; Hoffmann, C., Stein, A., Gallmann, E., Dörr, J., Krupitzer, C., Floto, H., Eds.; Gesellschaft für Informatik, Gesellschaft für Informatik (GI): Hohenheim-Stuttgart, Germany, 2024; pp. 251–256.
42. McMaster, G.S.; Smika, D.E. Estimation and Evaluation of Winter Wheat Phenology in the Central Great Plains. *Agric. For. Meteorol.* **1988**, *43*, 1–18. [CrossRef]
43. Jacott, C.N.; Boden, S.A. Feeling the Heat: Developmental and Molecular Responses of Wheat and Barley to High Ambient Temperatures. *J. Exp. Bot.* **2020**, *71*, 5740–5751. [CrossRef] [PubMed]
44. Derakhshan, A.; Bakhshandeh, A.; Siadat, S.A.-a.; Moradi-Telavat, M.R.; Andarzian, S.B. Quantifying the Germination Response of Spring Canola (*Brassica napus* L.) to Temperature. *Ind. Crops Prod.* **2018**, *122*, 195–201. [CrossRef]
45. TERRY, N. Developmental Physiology of Sugar Beet: I. The Influence of Light and Temperature on Growth. *J. Exp. Bot.* **1968**, *19*, 795–811. [CrossRef]
46. Radke, J.K.; Bauer, R.E. Growth of Sugar Beets as Affected by Root Temperatures Part I: Greenhouse Studies. *Agron. J.* **1969**, *61*, 860–863. [CrossRef]
47. Haverkort, A.J.; Verhagen, A. Climate Change and Its Repercussions for the Potato Supply Chain. *Potato Res.* **2008**, *51*, 223–237. [CrossRef]
48. Rykaczewska, K. The Effect of High Temperature Occurring in Subsequent Stages of Plant Development on Potato Yield and Tuber Physiological Defects. *Am. J. Potato Res.* **2015**, *92*, 339–349. [CrossRef]
49. Gerstmann, H.; Doktor, D.; Gläßer, C.; Möller, M. PHASE: A Geostatistical Model for the Kriging-Based Spatial Prediction of Crop Phenology Using Public Phenological and Climatological Observations. *Comput. Electron. Agric.* **2016**, *127*, 726–738. [CrossRef]
50. ESA. *Sentinel-1 User Handbook*; European Space Agency: Paris, France, 2013.
51. Truckenbrodt, J.; Cremer, F.; Eberle, J. PyroSAR—A Framework for Large-Scale SAR Satellite Data Processing. In Proceedings of the 2019 Conference on Big Data from Space, Munich, Germany, 19–21 February 2019.
52. Richards, J.A. *Remote Sensing with Imaging Radar*; Springer: Berlin/Heidelberg, Germany, 2009; ISBN 9780387765679.
53. Cloude, S.R.; Pottier, E. A Review of Target Decomposition Theorems in Radar Polarimetry. *IEEE Trans. Geosci. Remote Sens.* **1996**, *34*, 498–518. [CrossRef]
54. Zhang, Z.; Wang, C.; Zhang, H.; Tang, Y.; Liu, X. Analysis of Permafrost Region Coherence Variation in the Qinghai–Tibet Plateau with a High-Resolution TerraSAR-X Image. *Remote Sens.* **2018**, *10*, 298. [CrossRef]
55. Cleveland, W.S. Robust Locally Weighted Regression and Smoothing Scatterplots. *J. Am. Stat. Assoc.* **1979**, *74*, 829–836. [CrossRef]
56. Verbesselt, J.; Zeileis, A.; Herold, M. Near Real-Time Disturbance Detection Using Satellite Image Time Series. *Remote Sens. Environ.* **2012**, *123*, 98–108. [CrossRef]

57. Verbesselt, J.; Hyndman, R.; Zeileis, A.; Culvenor, D. Phenological Change Detection while Accounting for Abrupt and Gradual Trends in Satellite Image Time Series. *Remote Sens. Environ.* **2010**, *114*, 2970–2980. [CrossRef]
58. Löw, J.; Hill, S.; Thiel, M.; Ullmann, T.; Conrad, C. Tracking Crop Phenology across Different Sentinel-1 Orbits by Combining PolSAR Features with Growing Degree Data. In Proceedings of the DGPF-Jahrestagung 2024. Stadt, Land, Fluss—Daten vernetzen, Remagen, Germany, 13–14 March 2024; Kersten, T., Tilly, N., Eds.; pp. 342–355.
59. Veloso, A.; Mermoz, S.; Bouvet, A.; Le Toan, T.; Planells, M.; Dejoux, J.F.; Ceschia, E. Understanding the Temporal Behavior of Crops Using Sentinel-1 and Sentinel-2-like Data for Agricultural Applications. *Remote Sens. Environ.* **2017**, *199*, 415–426. [CrossRef]
60. García-Pedrero, A.; Gonzalo-Martín, C.; Lillo-Saavedra, M. A Machine Learning Approach for Agricultural Parcel Delineation through Agglomerative Segmentation. *Int. J. Remote Sens.* **2017**, *38*, 1809–1819. [CrossRef]
61. Tetteh, G.O.; Gocht, A.; Conrad, C. Optimal Parameters for Delineating Agricultural Parcels from Satellite Images Based on Supervised Bayesian Optimization. *Comput. Electron. Agric.* **2020**, *178*, 105696. [CrossRef]
62. Blickensdörfer, L.; Schwieder, M.; Pflugmacher, D.; Nendel, C.; Erasmi, S.; Hostert, P. Mapping of Crop Types and Crop Sequences with Combined Time Series of Sentinel-1, Sentinel-2 and Landsat 8 Data for Germany. *Remote Sens. Environ.* **2022**, *269*, 112831. [CrossRef]